Molecular Pharmacology Fast Forward. Published on April 29, 2019 as DOI: 10.1124/mol.118.115311
This article has not been copyedited and formatted. The final version may differ from this version.



# Impact of Phosphodiesterase 4 Inhibition on the Operational Efficacy, Response Maxima and Kinetics of Indacaterol-induced Gene Expression Changes in BEAS-2B Airway Epithelial Cells: A Global Transcriptomic Analysis

Radhika Joshi, Dong Yan, Omar Hamed, Mahmoud M. Mostafa, Taruna Joshi[1], Robert Newton & Mark A. Giembycz

*Departments of Physiology & Pharmacology (R.J., D.Y., O.H., T.J., M.A.G.) and Cell Biology & Anatomy (M.M.M., R.N.), Airways Inflammation Research Group, Snyder Institute for Chronic Diseases, Cumming School of Medicine, University of Calgary, Calgary, Alberta, Canada.*

Molecular Pharmacology Fast Forward. Published on April 29, 2019 as DOI: 10.1124/mol.118.115311
This article has not been copyedited and formatted. The final version may differ from this version.



**Running Head:** Genomic effects of PDE4 inhibitors in airway epithelia

**Corresponding Author:** Mark A. Giembycz PhD, Department of Physiology & Pharmacology, Airways Inflammation Research Group, Snyder Institute for Chronic Diseases, Cumming School of Medicine, University of Calgary, 3820 Hospital Drive N.W., Calgary, Alberta, Canada T2N 4N1. Telephone: (403) 210 8562; Fax: (403) 210 7944; e-mail: giembycz@ucalgary.ca

**Manuscript Information:**

Number of Text Pages (incl. References and Legends): **37**

Number of Tables: **1**

Number of Figures: **9**

Number of References: **63**

Number of words in Abstract: **250**

Number of words in Introduction: **659**

Number of words in Discussion: **1774**

**ABBREVIATIONS:** AE, adverse effect; ANOVA, analysis of variance; ASM, airways smooth muscle; $AUC_{0\text{-}18h}$, area under the curve from 0 to 18h; β2A, 8-hydroxy-5-((*R*)-1-hydroxy-2-methylaminoethyl)-1*H*-quinolin-2-one; COPD, chronic obstructive pulmonary disease; CRE, cAMP response element; CREB, cAMP response element binding protein; DAVID, database for visualization and integrated discovery; DCITC, 5(2-(((1′-(4′-isothiocyanatephenylamino)thiocarbonyl)amino)-2-methylpropyl) amino-2-hydroxypropoxy)-3,4-dihydrocarbostyril; DEGs, differentially-expressed genes; DMEM, Dulbecco's modified Eagle's medium; *E*, pharmacological effect; FCS, fetal calf serum; FDR, false discovery rate; GO, gene ontology; GSK 256066, 6-[3-(dimethylcarbamoyl)benzenesulphonyl]-4-[(3-methoxyphenyl)amino]-8-methylquinoline-3-carboxamide; HGNC, human genome nomenclature committee; ICS, inhaled corticosteroid; IL-6, interleukin-6; Ind+GSK, indacaterol and GSK 256066 in combination; KEGG, Kyoto encyclopedia of genes and genomes; LABA, long-acting $\beta_2$-adrenoceptor agonist; LAMA, long-acting muscarinic receptor antagonist; $n_H$, Hill coefficient; PDE, phosphodiesterase; RNO, roflumilast *N*-oxide; $Salm_{0.3}$, salmeterol 0.3nM; $Salm_{0.5}$, salmeterol 0.5nM; $Salm_{100}$, salmeterol 100nM; SFM, serum-free medium; TAC, transcriptome analysis console; TPM, transcripts per million.

Molecular Pharmacology Fast Forward. Published on April 29, 2019 as DOI: 10.1124/mol.118.115311
This article has not been copyedited and formatted. The final version may differ from this version.



## ABSTRACT

The effects of phosphodiesterase (PDE) 4 inhibitors on gene expression changes in BEAS-2B human airway epithelial cells are reported and discussed in relation to the mechanism(s) of action of roflumilast in chronic obstructive pulmonary disease (COPD). Microarray-based gene expression profiling failed to identify mRNA transcripts that were differentially regulated by the PDE4 inhibitor, GSK 256066 after 1, 2, 6 or 18h of exposure. However, real-time PCR analysis revealed that GSK 256066 was a weak stimulus and the negative microarray results reflected low statistical power due to small sample sizes. Furthermore, GSK 256066, roflumilast and its biologically-active metabolite, roflumilast *N*-oxide, generally potentiated gene expression changes produced by the long-acting $\beta_2$-adrenoceptor agonists (LABAs), salmeterol, indacaterol and formoterol. Many of these genes encode proteins with anti-viral, anti-inflammatory and anti-bacterial activities that could contribute to the clinical efficacy of roflumilast in COPD. RNA-Seq experiments established that the sensitivity of genes to salmeterol varied by ~7.5-fold. Consequently, the degree to which a PDE4 inhibitor potentiated the effect of a given concentration of LABA was gene dependent. Operational model fitting of concentration-response curve data from cells subjected to fractional, $\beta_2$-adrenoceptor inactivation determined that PDE4 inhibition increased the potency and doubled the efficacy of LABAs. Thus, adding-on roflumilast to standard triple therapy, as COPD guidelines recommend, may have clinical relevance especially in target tissues where LABAs behave as partial agonists. Collectively, these results suggest that the genomic impact of roflumilast, including its ability to augment LABA-induced gene expression changes, may contribute to its therapeutic activity in COPD.

Molecular Pharmacology Fast Forward. Published on April 29, 2019 as DOI: 10.1124/mol.118.115311
This article has not been copyedited and formatted. The final version may differ from this version.



## Introduction

Phosphodiesterase (PDE) 4 inhibitors entered clinical development in the 1980s as potential anti-depressant drugs (Zeller et al., 1984) and, since that time, have suffered a high level of attrition due to a low therapeutic ratio and weak efficacy (Giembycz, 2008). Nevertheless, in April 2010, roflumilast became the first, selective, orally-active, PDE4 inhibitor to be approved for human use with chronic obstructive pulmonary disease (COPD) being a primary indication (Giembycz and Field, 2010; Gross et al., 2010; Wedzicha et al., 2016). The 2019 Global Initiative for Chronic Obstructive Lung Disease guidelines recommend that roflumilast be used as an add-on therapy in a specific sub-group of patients with COPD. These are categorised as high risk, having severe, symptomatic disease in whom exacerbations occur despite regular treatment with a combination of a long-acting $\beta_2$-adrenoceptor agonist (LABA), a long-acting muscarinic receptor antagonist (LAMA) and an inhaled corticosteroid (ICS) (http://goldcopd.org). In this COPD phenotype, the therapeutic activity of roflumilast relies on its ability to improve airway calibre. However, PDE4 inhibitors do not promote acute bronchodilatation (Grootendorst et al., 2003), suggesting that the gain in lung function and associated reduction in exacerbation frequency are unrelated to direct airways smooth muscle (ASM) relaxation. Instead, preclinical studies and trials of roflumilast in human subjects suggest a primary mode of action is to suppress inflammation (Gamble et al., 2003; Giembycz and Newton, 2014; Grootendorst et al., 2007; Hatzelmann et al., 2010; Moodley et al., 2013).

Another selective, orally-active PDE4 inhibitor, apremilast, was approved in 2015 for the treatment of plaque psoriasis and psoriatic arthritis (Fala, 2015). Similar to the COPD phenotype for which roflumilast is indicated, these disorders are characterised by a chronic, systemic dysregulation of cytokine generation with attendant inflammation, implying that PDE4 inhibitors may share the same or a similar mechanism of action (Pincelli et al., 2018).

At a molecular level, inhibition of PDE4 increases the intracellular concentration of cAMP in target cells and tissues. While the downstream signalling pathways that ultimately lead to improved clinical outcomes are ill defined, cAMP is known to modulate gene expression by activating a family of transcription factors of which cAMP response element-binding protein (CREB) and activating

transcription factor-1 are prototypical examples (Zhang et al., 2005). Recently, we reported that the LABAs, indacaterol and salmeterol, promoted significant, and potentially beneficial, gene expression changes in BEAS-2B airway epithelial cells and human primary bronchial epithelia by mechanisms that involve canonical, Gsα/adenylyl cyclase/cAMP-dependent signalling (Yan et al., 2018). Therefore, logic dictates that PDE4 inhibitors may also provide clinical benefit by modulating gene expression (BinMahfouz et al., 2015; Giembycz and Maurice, 2014; Joshi et al., 2017; Moodley et al., 2013; Tannheimer et al., 2012). A genomic, anti-inflammatory mechanism of action also accommodates the likelihood that ASM is but one of several tissues that are therapeutic targets of orally-active PDE4 inhibitors. In this respect, the airway epithelium, which is considered a major player in COPD pathogenesis (Crystal, 2014), and extrapulmonary tissues including circulating leukocytes, the vascular endothelium and the bone marrow are attractive additional candidates. Indeed, the need for systemic exposure may help explain why PDE4 inhibitors developed for inhaled administration have, without exception, failed in clinical trials of COPD.

In this study, we hypothesised that PDE4 inhibitors work, in part, by genomic mechanisms and interact in additive or synergistic manner with LABAs. To test this idea, the transcriptomic signatures of two, highly selective PDE4 inhibitors, roflumilast *N*-oxide (RNO), the active metabolite of roflumilast (Hatzelmann et al., 2010), and GSK 256066 (6-[3-(dimethylcarbamoyl)benzenesulphonyl]-4-[(3-methoxyphenyl)amino]-8-methylquinoline-3-carboxamide; Tralau-Stewart et al., 2011) were obtained in BEAS-2B human airway epithelial cells treated alone and concurrently with a LABA. In addition, the impact of PDE4 inhibitors on the operational efficacy, magnitude of response and duration of action of LABA-induced gene expression changes was determined. BEAS-2B cells were selected for this investigation because they display gene expression profiles that mirror, to a large degree, those obtained in human primary bronchial epithelial cells treated with a variety of stimuli including LABAs (Yan et al., 2018).

Molecular Pharmacology Fast Forward. Published on April 29, 2019 as DOI: 10.1124/mol.118.115311
This article has not been copyedited and formatted. The final version may differ from this version.



## Materials and Methods

**Drugs and Reagents.** GSK 256066, indacaterol and β2A (8-hydroxy-5-((*R*)-1-hydroxy-2-methyl aminoethyl)-1*H*-quinolin-2-one) were provided by Gilead Sciences (Seattle, WA). Salmeterol and formoterol were donated by GlaxoSmithKline (Stevenage, UK) and AstraZeneca (Mölndal, Sweden), respectively. Roflumilast and RNO were from Nycomed (Konstanz, Germany). DCITC (5(2-(((1′-(4′-isothiocyanatephenylamino)thiocarbonyl)amino)-2-methylpropyl)amino-2-hydroxypropoxy)-3,4-di hydrocarbostyril) was a gift from Dr. Stephen Baker (University of Florida, FL). All drugs were dissolved in DMSO and diluted in serum-free medium (SFM). The highest concentration of DMSO used in these experiments (0.2% v/v) did not affect any output measured.

**Generation of a CRE Reporter in BEAS-2B Cells.** Cells were transfected with 8μg of plasmid DNA (pADneo2-C6-BGL) using Lipofectamine 2000 (Invitrogen, Burlington, ON, Canada) to generate 6×CRE BEAS-2B luciferase reporter cells as described previously (Meja et al., 2004).

**Submersion Culture of BEAS-2B Cells.** BEAS-2B cells were cultured under a 5% $CO_2$/air atmosphere at 37$^{o}$C in 12- or 24-well plastic plates (Corning Life Sciences, Lowell, MA) containing keratinocyte-SFM (ThermoFisher Scientific, Burlington Ontario) supplemented with epidermal growth factor (5ng/ml), bovine pituitary extract (50μg/ml), penicillin (100mg/ml) and streptomycin (100IU/ml). When confluent, cells were growth-arrested for 24h in keratinocyte-SFM without supplements (Greer et al., 2013) and processed as described below. For RNA-seq and subsequent validation experiments, BEAS-2B cells were grown in Dulbecco's modified Eagle's/Ham's F12 medium containing 10% fetal bovine serum, 2.5mM L-glutamine and 14mM $NaHCO_3$ (all Invitrogen) until confluent, and for a further 24h in SFM.

**Measurement of Luciferase Activity.** 6×CRE BEAS-2B reporter cells were treated with PDE4 inhibitor (GSK 256066, roflumilast or RNO) or LABA (indacaterol, salmeterol or formoterol) alone and in the combinations indicated in the text. After 6h, cells were lysed in 1× firefly luciferase buffer (Biotium, Hayward, CA) and luciferase activity was measured by luminometry. Data are expressed as fold increase in enzyme activity relative to vehicle-treated samples matched for time.

Molecular Pharmacology Fast Forward. Published on April 29, 2019 as DOI: 10.1124/mol.118.115311
This article has not been copyedited and formatted. The final version may differ from this version.



**Western Blot Analyses and ELISAs**. Confluent BEAS-2B cells at 37°C were incubated with RNO (1μM) and/or salmeterol (100nM). At 60min, the culture medium was decanted and cells were lysed in HCl (0.1M). cAMP in the resulting lysates was measured by ELISAs (Enzo Life Sciences, Farmingdale, NY) according to the manufacturer's instructions. Alternatively, cells were incubated with GSK 256066 and indacaterol alone and in combination at the concentrations indicated. At 6h supernatants were collected and interleukin-6 (IL-6) was measured by ELISA (D6050; R&D Systems, Minneapolis, MN). Cells were lysed in 1× Laemmli buffer supplemented with phosphatase inhibitors (Sigma-Aldrich) and 1× complete protease inhibitor cocktail (Roche, Indianapolis, IN). The cell lysates were size fractionated on 10% acrylamide gels, electrotransferred onto reinforced 0.2μM nitrocellulose membranes (GE Healthcare, Waukesha, WI) and blocked with 5% milk in Tris-buffered saline containing 1% Tween 20. Subsequently, membranes were probed with antibodies against NR4A2 (PP-N1404-00), NR4A3 (PP-H7833-00; both Perseus Proteomics Inc., Tokyo), and GAPDH (MCA4739; Bio-Rad, Hercules, CA). After washing, membranes were incubated with horseradish peroxidase-conjugated, anti-mouse immunoglobulin (115-035-003; Jackson ImmunoResearch Laboratories Inc., West Grove, PA). Proteins were detected by chemiluminescence using SuperSignal™ West Pico PLUS chemiluminescent substrate (#34580, ThermoFisher Scientific), visualized by autoradiography and expressed relative to GAPDH. Preliminary studies verified the identity of NR4A2 and NR4A3 by gene silencing (data not shown).

**Measurement of Gene Expression by Real-time PCR.** BEAS-2B cells were treated with PDE4 inhibitor and/or LABA as described above. Total RNA was extracted (RNeasy Mini Kit, Qiagen Inc., Mississauga, ON, Canada) and reverse transcribed using a qscript cDNA synthesis kit according to the manufacturer's instructions (Quanta Biosciences, Gaithersburg, MD). Real-time PCR analysis of cDNA was performed using the primer sequences shown in supplemental table 1 as described previously (Joshi et al., 2017; Yan et al., 2018).

**Gene Expression Profiling by Microarray.** BEAS-2B cells were cultured for 1, 2, 6 and 18h ($N$ = 4 at each time-point) with vehicle, GSK 256066 (10nM) and a concentration of indacaterol (10nM) that maximally activated 6×CRE reporter cells (Supplemental Fig. 1). Cells were also treated with

Molecular Pharmacology Fast Forward. Published on April 29, 2019 as DOI: 10.1124/mol.118.115311
This article has not been copyedited and formatted. The final version may differ from this version.



indacaterol and GSK 256066 in combination (Ind+GSK, both 10nM) under identical conditions. Total RNA was extracted (*vide supra*) and processed for gene expression profiling (Yan et al., 2018). The microarray images were scaled and normalised using the probe logarithmic intensity error algorithm in Transcriptome Analysis Console (TAC, *v*4.0; Affymetrix, Santa Clara, CA) and stored as .chp files. Signals from the four replicates for each probe set were averaged and the relative expression patterning was implemented in TAC. At each time-point, data from all treatments were analysed concurrently and visualized by generating volcano plots. The *P* statistic was adjusted using the Benjamini and Hochberg false discovery rate (FDR), with step-up procedure, and significance was set to the <0.1, <0.05 and <0.01 probability levels as indicated.

**Gene Expression Profiling by RNA-Seq.** BEAS-2B cells were treated for 2h with vehicle, RNO (1μM) and two, submaximal concentrations of salmeterol (0.3nM [$Salm_{0.3}$] and 0.5nM [$Salm_{0.5}$]) alone and in the presence of RNO (1μM). A maximally-effective concentration of salmeterol (100nM, $Salm_{100}$) was examined in parallel to define maximum responses. Total RNA was extracted as described above and a total of 28 samples ($N$ = 4 per treatment group) were submitted to the Centre for Health Genomics and Informatics, University of Calgary, for sequencing.

RNA sequencing libraries were prepared using the NEBNext Ultra II Directional kit (New England Biolabs, Ipswich, MA) with the poly(A) mRNA magnetic isolation module as described by the manufacturer. The libraries were validated by using the D1000 Screen Tape assay on an Agilent 2200 TapeStation system (Agilent Technologies, Santa Clara, CA) and quantified with a Kapa qPCR Library Quantification kit for Illumina (Kapa Biosystems, Boston, MA). The libraries were pooled and sequenced across two consecutive, single end, 75 cycle sequencing runs on a NextSeq 500 instrument (Illumina, San Diego, CA) according to the manufacturer's instructions, generating approximately 33 million reads per sample.

Demultiplexing of the sequencing data and read quality of each sample were performed using bcl2fastq conversion software (*v*2.18.0.12, Illumina) and FastQC (*v*0.10.1) respectively. Good-quality reads were mapped to the reference human transcriptome (GRCh37/hg19 version) and quantified by using Kallisto

Molecular Pharmacology Fast Forward. Published on April 29, 2019 as DOI: 10.1124/mol.118.115311
This article has not been copyedited and formatted. The final version may differ from this version.



(*v*0.42.4) (Bray et al., 2016) with 100 bootstraps per sample. Differential expression analysis was performed at the transcript and gene level using the *R* package, Sleuth (*v*0.30.0) (Pimentel et al., 2017). Pairwise comparisons were performed between vehicle- and salmeterol (100nM)-treated samples, and differentially-expressed genes (DEGs) were identified based on a FDR-corrected *P* value of ≤0.05. Induced (≥2-fold) and repressed (≤0.5-fold) genes were filtered to remove those expressed at ≤1 transcript per million (TPM) after $Salm_{100}$ and vehicle, respectively before subsequent analyses. Pairwise comparisons of these DEGs were performed between vehicle and all other treatments using the Wald test in Sleuth to estimate fold changes (derived from beta-values). Data were also expressed as a change in TPM as indicated.

**Analysis of Gene Expression Profiles.** The microarray and RNA-seq data have been deposited with NCBI's Gene Expression Omnibus and are freely available using accession codes GSE106710 and GSE126981 respectively. Unless stated otherwise, genes are referred to by the official human genome nomenclature committee (HGNC) symbols supplied by the National Center for Biotechnology Information (www.ncbi.nlm.nih.gov). Functional annotation clustering of indacaterol- and Ind+GSK-regulated genes including associated enriched gene ontology (GO) terms was performed with the database for visualization and integrated discovery (DAVID) bioinformatics resources (*v*6.8) at medium stringency (Huang et al., 2009). Results are reported using the GO term that describes biological process (GOTERM_BP_DIRECT). When this descriptor was absent from a given gene cluster, molecular function (GOTERM_MF_DIRECT), cellular component (GOTERM_CC_DIRECT), UniProt Sequence Feature, Uniprot Key Word, InterPro or Kyoto Encyclopedia of Genes and Genomes (KEGG) pathway was reported. Pseudogenes, hypothetical genes, noncoding RNAs and uncharacterised sequences lacking annotation were excluded from all analyses.

**Curve Fitting.** Monophasic *E*/[A] curves were fit by least-squares, non-linear, iterative regression to the following form of the Hill equation (Eq. 1; Prism 6®, GraphPad Software Inc, San Diego, CA):

$$E = E_{min} + \frac{(E_{max} - E_{min})}{1 + 10^{(p[A]_{50} - p[A])^{n_H}}} \qquad \text{(Eq. 1)}$$

Molecular Pharmacology Fast Forward. Published on April 29, 2019 as DOI: 10.1124/mol.118.115311
This article has not been copyedited and formatted. The final version may differ from this version.



where $E$ is the pharmacological effect, $E_{min}$ and $E_{max}$ are the basal response and maximum response respectively, p[A] is the negative log molar concentration of the compound of interest, $p[A]_{50}$ is a location parameter equal to the negative log molar concentration of compound producing ($E_{max}$ - $E_{min}$)/2 and $n_H$ is the Hill coefficient of the $E$/[A] curve at the $p[A]_{50}$ level.

**Applying Fractional Receptor Depletion to Quantify the Impact of PDE4 Inhibition on the Efficacy of $\beta_2$-Adrenoceptor Agonists.** $E$/[A] curves were constructed to salmeterol and β2A, a quinolinone-based orthostere (Yoshizaki et al., 1976) present in many $\beta_2$-adrenoceptor agonists, in the absence and presence of a PDE4 inhibitor. These experiments were performed in cells that had been pre-treated (60min) with vehicle or the alkylating agent, DCITC (100nM) and then washed in SFM (Deyrup et al., 1998). Each family of $E$/[A] curves was fit simultaneously to the operational model of agonism (Eq. 2), which describes a theoretical relationship between $E$ and agonist concentration (Black and Leff, 1983). Algebraically,

$$E = \frac{E_m.\tau^n.[A]^n}{(K_A + [A])^n + \tau^n.[A]^n} \qquad \text{(Eq. 2)}$$

where $E_m$ is the theoretical maximum response of the tissue, $K_A$ is the agonist equilibrium dissociation constant, [A] is agonist concentration, $n$ is the slope of the relationship between the concentration of agonist-receptor complexes and response, and τ is the operational efficacy of the agonist. In these analyses, only τ was allowed to vary between individual $E$/[A] curves; for all other parameters (i.e., $E_m$, $K_A$ and $n$) a common value was assumed (Black and Leff, 1983; Leff et al., 1990).

**Determination of Receptor Reserve.** Occupancy-response curves in the absence and presence of a PDE4 inhibitor were constructed using $K_A$ values determined by $\beta_2$-adrenoceptor depletion. At each concentration of agonist, fractional receptor occupancy was determined assuming the binding of ligand to the $\beta_2$-adrenoceptor was a non-cooperative process (Eq. 3) where $R_A$ and $R_t$ represent the number of agonist-occupied receptors and total number of receptors respectively.

$$R_A/R_t = [A]/(K_A + [A]) \qquad \text{(Eq. 3)}$$

**Statistics.** Data are presented as the mean ± s.e. mean or as Box and Whisker plots of $N$ independent

Molecular Pharmacology Fast Forward. Published on April 29, 2019 as DOI: 10.1124/mol.118.115311
This article has not been copyedited and formatted. The final version may differ from this version.



determinations. Differences in CRE reporter activity and gene expression changes were evaluated by using Student's *t*-test or repeated measures, one-way ANOVA as indicated. When the ANOVA *F*-test *P* value was <0.05, differences between groups were identified by using Tukey's multiple comparison test without Greenhouse-Geisser correction (Lew, 2007). The relationship between global changes in gene expression produced by two treatment interventions was determined by Pearson product moment correlation. Least squared perpendicular major axis (Deming) regression (Cornbleet and Gochman, 1979) was used to verify differences between treatments or treatment methods. In the text, the terms *synergy* and *synergistic* refer to a change in gene expression produced by a LABA and a PDE4 inhibitor in combination that is greater than the sum of their individual effects. The null hypothesis was rejected when $P<0.05$.

Molecular Pharmacology Fast Forward. Published on April 29, 2019 as DOI: 10.1124/mol.118.115311
This article has not been copyedited and formatted. The final version may differ from this version.



## Results

**Effect of GSK 256066 on Global Gene Expression Changes.** The microarray results of GSK 256066-treated BEAS-2B cells are displayed as volcano plots in supplemental figure 2 where induced and repressed genes are represented as red circles (>1.5-fold) and blue circles (<0.67-fold) respectively. Although many gene expression changes were apparent, and exceeded *P* values of 0.05 obtained by ANOVA, no probe set on the array was significantly different from vehicle at a Benjamini and Hochberg FDR of <10%. Previously, we reported that PDE4 inhibitors can potentiate LABA-induced gene expression in BEAS-2B cells suggesting that a common pool of cAMP may regulate transcription (BinMahfouz et al., 2015; Moodley et al., 2013). Thus, these results reported here may indicate that GSK 256066 is a weak stimulus in these cells and that the small sample size lacked statistical power. To address this prospect, indacaterol (10nM)-regulated gene expression changes at 1, 2 and 6h were correlated against their counterparts in GSK 256066-treated BEAS-2B cells using FDRs of <10%, <5% and <1% (Fig. 1A). This approach revealed significant correlations between the two drugs, which strengthened as the stringency of the FDR was increased. Furthermore, slopes of Deming regressions were shallow (0.23-0.36) at all time-points, which is consistent with weak transcriptional activity of GSK 256066 relative to indacaterol. Using the same RNA, the expression of 18 genes (labelled A to R) that were significantly (FDR <5%) up-regulated by indacaterol at 2h (yellow circles in figure 1 and supplemental figure 2) were tested for their sensitivity to GSK 256066 by real-time PCR. These results are shown in supplemental figure 3 where the expression of each gene is plotted over time together with data from the probe set that gave the most robust increase on the microarray. Pearson's analyses indicated significant correlations between the microarray- and PCR-generated data at 1, 2 and 6h (Fig. 1B) although changes in gene expression were modest and did not reach statistical significance (Supplemental Fig. 3). However, repeating this experiment with a larger sample size established that most of these genes were significantly upregulated in BEAS-2B cells exposed to GSK 256066 (10nM) and roflumilast (1μM) for 1 and/or 2h (Supplemental Fig. 4).

**Effect of GSK 256066 on Expression of the Indacaterol-regulated Transcriptome.** Microarrays were also used to determine the effect of GSK 256066 (10nM) on the *number* of genes that were

Molecular Pharmacology Fast Forward. Published on April 29, 2019 as DOI: 10.1124/mol.118.115311
This article has not been copyedited and formatted. The final version may differ from this version.



significantly (FDR <10%) induced or repressed at 1, 2, 6 and 18h (Fig. 2A) by a concentration of indacaterol (10nM) that maximally activated 6×CRE reporter cells (Supplemental Fig. 1). Relative to time-matched, vehicle-treated cells, 181 DEGs were either up-regulated (135) or down-regulated (46) at 1h by >1.5-fold and <0.67-fold respectively. At 2h, the number of DEGs had increased to 351 (304 induced and 47 repressed), which had declined to 251 (206 induced and 45 repressed) by 6h. At 18h, 9 genes were up-regulated and 1 gene was down-regulated by indacaterol.

In the presence of GSK 256066, the number of indacaterol-regulated genes at 1 and 2h was similar to the gene count in BEAS-2B cells exposed to indacaterol alone (Fig. 2A). In contrast, at 6 and 18h the number of significant gene expression changes was considerably greater in cells exposed to Ind+GSK than to indacaterol (Fig. 2A). The Venn diagrams in figure 2B show that 41, 87, 86 and 60% of all genes induced or repressed by indacaterol were similarly regulated by Ind+GSK at 1, 2, 6 and 18h respectively. The corresponding values for genes induced or repressed by Ind+GSK that were also regulated by indacaterol were 56, 86, 55 and 30%. Analyses of data at all time-points revealed that ≥70% of all genes were regulated by both interventions (Fig. 2B).

**Ontological Analysis and Functional Annotation Clustering.** Categorization of indacaterol- and Ind+GSK-regulated transcripts (by probe set) at 1, 2, 6 and 18h was performed manually using six generic descriptors: (**1**) *transcriptional regulators* (red); (**2**) *transporters, ion channels and membrane receptors* (orange); (**3**) *metabolic proteins* (yellow); (**4**) *general signalling molecules, including translational regulators* (green); (**5**) *other functions* (blue); and (**6**) *not assigned* (purple). Annotated probe sets meeting the expression criteria (>1.5-fold, <0.67-fold; FDR <10%) were assigned HGNC gene symbols and are listed in supplemental tables 2 and 3. The number of induced and repressed genes within each general terms expressed as a percentage of the total number of significant gene expression changes is also presented as a pie chart at each time-point for each intervention.

To explore how downstream function may change with time, the number of DEGs assigned to each of the six terms described above was enumerated at 1, 2, 6 and 18h (Supplemental Fig. 5). Apart from repressed genes assigned to the term *receptors, ion channels and transporters*, the gene count in each

Molecular Pharmacology Fast Forward. Published on April 29, 2019 as DOI: 10.1124/mol.118.115311
This article has not been copyedited and formatted. The final version may differ from this version.



of the other categories mirrored the global effect of GSK 256066 on the indacaterol-regulated transcriptome (Fig. 2A). Breaking down these changes by category showed that indacaterol promoted a transient burst (peaking at 2h) in induced and repressed genes that are associated with transcriptional regulation and signalling. At 1, 2 and 18h the gene count was not materially affected by GSK 256066 whereas at 6h it was markedly increased (Supplemental Fig. 5). Indacaterol-regulated gene expression changes in the other categories occurred more slowly with the highest number recorded at 6h. Again, GSK 256066 did not affect the number of DEGs at the early or late time-points; only those appearing at 6h were increased in number (Supplemental Fig. 5).

Functional annotation clustering of genes that were differentially expressed in response to indacaterol and Ind+GSK across all time-points determined that the number of clusters and enriched GO terms within each cluster were similar (Supplemental Tables 4 & 5). Many of the most highly enriched terms, such as *positive regulation of transcription from RNA polymerase II promoter* (GO:0045944), relate to gene transcription and contain transcripts that encode sequence-specific transcription factors, co-activators, (co)repressors and allied regulators of gene expression. Of these, several encode transcriptional repressors including *KLF2*, *KLF4*, *KLF15*, *NR4A1*, *NR4A2* and *NR4A3*. Other enriched GO terms such as *transcription, DNA templated* (GO:0006351), *extracellular region* (GO:0005576), *integral component of plasma membrane* (GO:0005887), *peptidyl-threonine dephosphorylation* (GO:0035970) and *type I interferon signaling pathway* (GO:0060337) contained genes that may attenuate cytokine production (*CD200*, *DUSP1*, *SOC3*), protect against COPD exacerbations (*DMBT1*, *CRISPLD2*) and regulate oxidative stress, fibrosis and mucus secretion (*EGR1*, *TXNIP*).

Enriched GO and KEGG terms including *extracellular space* (GO:0005615), *cell-cell signaling* (GO:0007267), *cytokine activity* (GO:0005125), *positive regulation of tyrosine phosphorylation of stat3 protein* (GO:0042531) and *TNF signalling pathway* (HSA:04688) were populated with a variety of adverse effect (AE) genes notably *AREG*, *BDNF*, *CCL2*, *CCL20*, *CXCL2*, *CXCL3*, *CTGF*, *EDN1*, *IL6*, *IL11*, *IL15* and *IL20*.

Molecular Pharmacology Fast Forward. Published on April 29, 2019 as DOI: 10.1124/mol.118.115311
This article has not been copyedited and formatted. The final version may differ from this version.



A comprehensive analysis of indacaterol-regulated transcripts in BEAS-2B cells including functional annotation clustering has been reported previously (Yan et al., 2018) and those findings were largely replicated here in BEAS-2B cells treated with Ind+GSK (Supplemental Tables 2-5).

**Effect of GSK 256066 on the Duration of Indacaterol-induced Gene Expression Changes.** The global effect of PDE4 inhibition on the expression of the indacaterol-regulated transcriptome was further interrogated by comparing the magnitudes of all significant gene expression changes (by probe set) induced by Ind+GSK at 1, 2, 6 and 18h (no fold threshold at the FDR indicated) with the corresponding indacaterol data (Fig. 3). This analysis revealed significant correlations between the two treatments at each time-point. At 1 and 2h, GSK 256066 had little effect on those genes up-regulated by indacaterol (slopes of Deming regressions ~1) whereas at the two later time-points slopes of regressions were shallow in favour of Ind+GSK (Fig. 3C & D). The overall effect of this interaction is presented in figure 3E-H as areas under the curves of the mean change in gene expression over the total period of exposure ($AUC_{0\text{-}18h}$). For example, taking the 158 probe sets that were significantly upregulated by Ind+GSK at 1h, plotting the overall mean induction of the same probe sets at 2, 6 and 18h, and comparing these results with the indacaterol counterparts (Fig. 3E), revealed that GSK 256066 produced an overall enhancement of gene induction. Similar data were obtained for those genes significantly up-regulated by Ind+GSK at the other time-points (Fig. 3F-H). These outcomes were attributable to the persistence of gene expression changes at 1 and 2h, as well as the induction of a greater number of genes at 6 and 18h. In each case, the $AUC_{0\text{-}18h}$ for the 1, 2, 6 and 18h data sets was 23, 21, 20 and 28% greater in cells treated with Ind+GSK compared to indacaterol alone respectively (Fig. 3E-H). Indacaterol-repressed genes were affected similarly (Supplemental Fig. 6).

The impact of GSK 256066 on the $AUC_{0\text{-}18h}$ of the 259 probe sets that were significantly induced (>2-fold; FDR <10%) by indacaterol at any time-point was converted to a fold change and presented as a heat map. As shown in figure 4, the effects of PDE4 inhibition were gene-dependent and formed a continuum that ranged from 2.5-fold for *DNAI1* to 0.21-fold for *UGT1A8/9*. Using cut-off levels of >1.1-fold and <0.9-fold, GSK 256066 variably increased and decreased respectively $AUC_{0\text{-}18h}$ of 157

Molecular Pharmacology Fast Forward. Published on April 29, 2019 as DOI: 10.1124/mol.118.115311
This article has not been copyedited and formatted. The final version may differ from this version.



(61%) and 34 (13%) indacaterol-induced transcripts. The $AUC_{0\text{-}18h}$ of the remaining 68 (26%) transcripts were unaffected (Fig. 4).

The effects of GSK 256066 on 18 indacaterol-induced genes (labelled A to R in figure 4) that spanned $AUC_{0\text{-}18h}$ continuum were validated by real-time PCR using the same RNA (Fig. 5). For the majority (13/18) of these genes, GSK 256066 variably enhanced the indacaterol $AUC_{0\text{-}18h}$ by maintaining transcript expression at the 6 and 18h time-points. However, the kinetics of other gene expression changes (i.e., *C5AR1, CRISPLD2, DMBT1, SOCS3*) were unaffected by GSK 256066 or even abbreviated (e.g. *BMP2*), which suggests gene-dependent differences in regulation by cAMP.

**Effect of PDE4 Inhibition on the Magnitude of Gene Expression Changes produced by a Submaximal Concentration of a LABA.** The experiments described in the previous section explored the impact of RNO in cells treated with a maximally-effective concentration of indacaterol (10nM; Supplemental Fig. 1). As this may have precluded an assessment of whether these drugs could interact in an additive or synergistic manner, the effects of a lower concentration of indacaterol (1nM; $[A]_{32}$) on the expression of nine genes was determined in the absence and presence of GSK 256066 (10nM) and roflumilast (1μM). In most cases, at 1 and/or 2h, the effect of the drugs in combination was greater than the LABA alone (Fig. 6A). When changes in expression produced by the drugs in combination were plotted against the sum of their individual effects, lines of Deming regressions deviated from unity raising the possibility that the PDE4 inhibitor and LABA interacted synergistically (Fig. 6B). A similar and more striking interaction occurred when indacaterol was substituted with a higher effective concentration of formoterol (30pM; $[A]_{45}$; Fig, 6A & B). These data are also presented as Box and Whisker plots to illustrate the variability in response to LABA and PDE4 inhibitor (Supplemental Fig. 4). The ability of GSK 256066 to enhance the effect of indacaterol was reproduced at the protein level using NR4A2, NR4A3 and IL-6 as representative examples (Fig. 6C).

**The Salmeterol-Regulated Transcriptome and the Effect of RNO.** RNA-seq was used to establish if PDE4 inhibitors augmented the expression of all LABA-regulated genes or a subpopulation. For these experiments, RNO and salmeterol were substituted for GSK 256066 and indacaterol to provide clinical

Molecular Pharmacology Fast Forward. Published on April 29, 2019 as DOI: 10.1124/mol.118.115311
This article has not been copyedited and formatted. The final version may differ from this version.



applicability and to gain further evidence that this interaction represents a class effect of LABAs and PDE4 inhibitors. Initially, the sensitivity of genes that comprise the LABA-regulated transcriptome to agonist was determined. This was achieved by comparing global gene expression changes in BEAS-2B cells treated for 2h with two, submaximal concentrations of salmeterol ($Salm_{0.3}$ and $Salm_{0.5}$), which equated to a $[A]_{14}$ and $[A]_{36}$ on the 6×CRE reporter respectively, with a concentration of salmeterol (100nM; $Salm_{100}$) that defined maximal responses (Supplemental Fig. 1).

At a FDR of ≤5%, 180 and 16 genes were significantly induced (≥2-fold) and repressed (≤0.5-fold) respectively by $Salm_{100}$. Changes in gene expression produced by $Salm_{0.3}$ expressed as a percentage of the corresponding $Salm_{100}$ data formed a continuum that ranged from 11.6% (*NPTX1*) to 83% (*TCF21*) for up-regulated genes (Fig. 7A), and from 37.6% (*C10orf10*) to 71.6% (*KRTAP2-3/KRTAP2-4*) for genes that were repressed (Supplemental Table 7). Assuming that (i) salmeterol is a full agonist on all DEGs; (ii) gene expression is described by symmetrical *E*/[A] curves with $n_H$ = 1.8 (Supplemental Fig. 1); and (iii) $Salm_{100}$ maximally induced or repressed all DEGs, then the sensitivity of genes within the salmeterol-regulated transcriptome varied by ~7.5-fold (Fig. 7A & B). In contrast, $Salm_{0.5}$ was a strong stimulus in BEAS-2B cells and, unlike its modest effect on the 6×CRE reporter (Supplemental Fig. 1), promoted gene expression changes that were ≥58% of their respective maxima (Fig. 7A).

In BEAS-2B cells treated for 2h with RNO (1μM), 16 genes were differentially regulated (≥2-fold; ≤0.5-fold; FDR ≤5%) consistent with the superior sensitivity of RNA-seq over microarrays. Analysis of the 196 $Salm_{100}$-regulated genes (Supplemental Table 7) revealed strong correlations between gene expression changes produced by RNO and all concentrations of salmeterol tested (Supplemental Fig. 7). The additional finding that RNO augmented salmeterol-induced cAMP accumulation (Fig. 7C) implies that both drugs can regulate gene expression by a common mechanism that involves the activation of PKA (Yan et al., 2018). To explore that possibility, gene expression changes produced by salmeterol and RNO in combination and the sum of their individual effects were analysed by Deming regression (Fig. 8A & B). On most genes, the activity of salmeterol was augmented by RNO (1μM) in a synergistic manner, which was reflected by slopes that were steeper than the line-of-identity in favour of $Salm_{0.3}$ + RNO (1.98) and $Salm_{0.5}$ + RNO (1.24; Fig. 8A & B). However, the magnitudes of these

Molecular Pharmacology Fast Forward. Published on April 29, 2019 as DOI: 10.1124/mol.118.115311
This article has not been copyedited and formatted. The final version may differ from this version.



interactions varied and formed a continuum due to differences in the sensitivity of genes to salmeterol (Supplemental Tables 7 & 8). This is illustrated in figure 8C & D, which shows simulated salmeterol *E*/[A] curves with $n_H$ fixed to a value of 1.8 (*vide supra*) in the absence and presence of a concentration of RNO that displaced the control curve three-fold to the left. It can be seen that the degree to which RNO augments a given response depends where on the salmeterol *E*/[A] curve the measurement is made and how it is calculated. On *NPTX1* and *TCF21,* which lie towards the extremes of the salmeterol sensitivity spectrum (Fig.7A), the impact of RNO differed markedly (Fig 8E & F). Thus, RNO augmented $Salm_{0.3}$-induced *NPTX1* and *TCF21* expression from 11.6 to 51% and from 83 to 97% of their maximum responses respectively.

**Quantifying the Impact of RNO on the Efficacy of Salmeterol.** Pre-treatment of 6×CRE BEAS-2B cells with RNO (1μM; 30 min) produced a modest activation of the reporter (<2-fold) and a 4.5-fold sinistral displacement of the mean salmeterol *E*/[A] curve without affecting the maximum response (Fig 9A). To mimic a therapeutic target where receptor number is limiting, the effect of RNO was examined in cells subjected to fractional, irreversible $\beta_2$-adrenoceptor inactivation with DCITC (100nM; 60 min). In these experiments, the upper asymptote of the mean *E*/[A] curve was significantly depressed (by 49%) and the potency of salmeterol was reduced by a factor of 8.5-fold. In the presence of RNO, the effects of receptor depletion were partially rescued; there was an increase in the potency of salmeterol and in the maximum response attained (Fig. 9A). Analysing this family of *E*/[A] curves by operational model fitting determined that RNO had doubled the efficacy of salmeterol in the absence ($\tau$: from 10.5 to 24) and presence ($\tau$': from 0.9 to 1.7) of DCITC (Table 1).

The operational model also provides a measure of agonist affinity. For salmeterol-induced reporter activation, this was calculated to be 3.7nM (Table 1). Substituting this value in to equation 3, which is a statement of the *Law of Mass Action,* provides a description of the relationship between receptor occupancy and response (Kenakin, 2016). For activation of 6×CRE BEAS-2B reporter cells, this relationship deviated significantly from the line-of-identity (Fig. 9B). Interpolation from the mean occupancy-response curve showed that 4, 13 and 25% receptor occupancy was required to generate 20, 50 and 80% of the maximal response, respectively and is consistent with a receptor reserve. In the

Molecular Pharmacology Fast Forward. Published on April 29, 2019 as DOI: 10.1124/mol.118.115311
This article has not been copyedited and formatted. The final version may differ from this version.



presence of RNO, the deviation from linearity was more pronounced; the salmeterol $K_A/[A]_{50}$ value was increased from 8 to 32 and the generation of 20, 50 and 80% of the maximal response now required only 1, 4 and 13% $\beta_2$-adrenoceptor occupancy, respectively (Fig. 9B).

In cells treated with DCITC, salmeterol-induced reporter activation collapsed to a linear function of receptor occupancy. The $K_A/[A']_{50}$ value was ~1 and the receptor reserve present under control conditions was lost (Fig. 9B). In contrast, the sensitivity of receptor-depleted cells treated with RNO to salmeterol was partially restored. The occupancy-response relationship returned to a shallow rectangular hyperbola, where 15, 43 and 77% binding generated 20, 50 and 80% of the maximal response respectively, and the $K_A/[A']_{50}$ value was increased from 0.74 to 1.59 (Fig. 9B; Table 1).

GSK 256066 (10nM; 30min) had a similar impact on the operational efficacy and receptor reserve of β2A (Fig. 9C & D; Table 1), the functionality that confers $\beta_2$-adrenoceptor agonism (Yoshizaki et al., 1976) in indacaterol, carmoterol and abediterol. Thus, the interaction between salmeterol and RNO shown in figure 9A is likely to be generic to LABAs and PDE4 inhibitors.

On *bona fide* genes (i.e., *CRISPLD2*, *NR4A2*, *RGS2*), RNO produced sinistral displacements of the salmeterol *E*/[A] curves in the absence and presence of DCITC consistent with increases in efficacy and receptor reserves (Fig. 9E-G). However, the quality of the data was not sufficiently robust for quantification by operational model fitting.

Molecular Pharmacology Fast Forward. Published on April 29, 2019 as DOI: 10.1124/mol.118.115311
This article has not been copyedited and formatted. The final version may differ from this version.



## Discussion

The results of large scale, phase III clinical trials indicate that the PDE4 inhibitor, roflumilast, is beneficial in a subset of individuals with severe, bronchitic COPD in whom frequent exacerbations occur despite ICS/LABA combination therapy, even in the presence of a LAMA. These results are important because they illustrate that the ceiling of benefit, following an additional drug intervention, had not been attained (Martinez et al., 2015; Martinez et al., 2018). While the mechanism of action of roflumilast is unclear, its ability to improve lung function and reduce exacerbation frequency (Wedzicha et al., 2016), in the absence of direct bronchodilatation (Grootendorst et al., 2003), implies that suppression of inflammation plays a role (Gamble et al., 2003; Grootendorst et al., 2007). We have reported previously that LABAs promote changes in gene expression in human airway epithelial cells that may contribute to: (i) their clinical efficacy in obstructive lung diseases, especially when combined with an ICS (Giembycz and Newton, 2011; Giembycz and Newton, 2015; Rider et al., 2018), and (ii) the AEs that are associated with chronic $\beta_2$-adrenoceptor agonist monotherapy (*vide infra*; Yan et al., 2018). This study extends those findings by establishing that PDE4 inhibitors also promoted changes in gene expression in BEAS-2B cells and, perhaps more importantly, increased the operational efficacy, enhanced the magnitude of response and variably altered gene expression kinetics induced by LABAs. Thus, if suppression of airways inflammation underpins the clinical activity of PDE4 inhibitors in COPD, genomic mechanisms may be involved.

**The PDE4-Regulated Transcriptome**. Immediate and delayed targets of cAMP signalling could equally contribute to the efficacy of PDE4 inhibitors. Accordingly, DEGs were identified in BEAS-2B cells exposed to GSK 256066 for 1, 2, 6 and 18h. GSK 256066 was chosen for this experiment because it is a potent, pan-PDE4 inhibitor with considerable selectivity (>30,000-fold) over all other PDE families and the *Cerep*® panel of receptors (Tralau-Stewart et al., 2011). At a concentration 3800× greater than its $K_I$ for the inhibition of human PDE4B1 (Joshi et al., 2017), GSK 256066 did not affect gene expression even at a FDR <10%. While these data suggested that genomic mechanisms play little role in the mechanism of action of PDE4 inhibitors, further analyses ascertained that GSK 256066 was a weak stimulus in BEAS-2B cells and the small sample size used for the arrays lacked statistical

Molecular Pharmacology Fast Forward. Published on April 29, 2019 as DOI: 10.1124/mol.118.115311
This article has not been copyedited and formatted. The final version may differ from this version.



power to detect small changes in gene expression. Indeed, real-time PCR confirmed that many genes induced by indacaterol were also up-regulated by GSK 256066 and roflumilast.

The weak transcriptional activity of PDE4 inhibitors may reflect low basal adenylyl cyclase activity in BEAS-2B cells and questions the significance of genomic mechanisms *in vivo*. This is an important consideration given that roflumilast monotherapy was beneficial in clinical trials of COPD (Calverley et al., 2009). However, the modest *in vitro* effects described here are likely amplified *in vivo* because adenylyl cyclase activity in target cells and tissues will be higher. Indeed, many Gs-coupled receptors will be under tonic activation by various endogenous ligands including catecholamines, adenosine and prostaglandins (BinMahfouz et al., 2015; Greer et al., 2013; Kaur et al., 2008; Moodley et al., 2013; Wilson et al., 2009). Furthermore, any genomic effects of PDE4 inhibitors could be further enhanced by endogenous glucocorticoids given that these drugs can often summate or even synergise at a transcriptional level (BinMahfouz et al., 2015; Moodley et al., 2013). Thus, the clinical efficacy of roflumilast monotherapy may reflect its ability to enhance the activity of various endogenous ligands to produce a more robust gene expression signature than these *in vitro* data suggest.

**Effect of PDE4 Inhibition on the LABA-Regulated Transcriptome**. Consistent with this *in vivo* prediction, RNO and GSK 256066 enhanced the expression of a panel of formoterol- and indacaterol-induced genes in BEAS-2B cells and this was reproduced at the protein level using NR4A2, NR4A3 and IL-6 as representative examples. Operational model fitting determined that PDE4 inhibition doubled the efficacy of LABAs and, thereby, increased the $\beta_2$-adrenoceptor reserve. Clinically, this finding could be described as “LABA sparing” where, in the presence of a PDE4 inhibitor, a lower agonist concentration is required to produce the same degree of gene induction or repression. To establish if this interaction extended to the LABA-regulated transcriptome or a subpopulation of DEGs, the effects of RNO on global gene expression changes produced by submaximal concentrations of salmeterol were determined by RNA-seq. In these experiments, RNO augmented the expression of the majority of DEGs. These included those with AE and therapeutic potential (*vide infra*), although the magnitude of effect varied because of the estimated 7.5-fold difference in their sensitivity to salmeterol. This was defined by *NPTX1* and *TCF21*, which lie towards the extremes of the sensitivity spectrum.

Molecular Pharmacology Fast Forward. Published on April 29, 2019 as DOI: 10.1124/mol.118.115311
This article has not been copyedited and formatted. The final version may differ from this version.



Thus, $Salm_{0.3}$ alone and in the presence of RNO equated respectively to $[A]_{11.6}$ and $[A]_{51}$ for *NPTX1* and $[A]_{83}$ and $[A]_{97}$ for *TCF21*. Collectively, these results support the idea that Gs-dependent signalling plays a dominant role in regulating $\beta_2$-adrenoceptor-mediated gene expression. While non-canonical mechanisms cannot be excluded (see Penn et al., 2013), *cis*-acting CREs for the transcription factor, CREB are found in the promoter regions of a large number of cAMP-regulated genes, which support this proposal (Zhang et al., 2005). An additive or synergistic interaction of a PDE4 inhibitor with a LABA may be particularly important in target cells and tissues that express low $\beta_2$-adrenoceptor number or where receptor-effector coupling efficiency is weak (Rabe et al., 1993). Indeed, modelling this scenario by rendering salmeterol and β2A (the functionality that confers agonism in many LABAs) partial agonists with DCITC, revealed that PDE4 inhibitors partially rescued the associated loss in operational efficacy, increased the maximum response and produced sinistral displacements of LABA *E*/[A] curves as the *Law of Mass Action* predicts.

GSK 256066 also prolonged the duration of many indacaterol-induced gene expression changes. This was prominent at 6h and often persisted to 18h when the level of mRNA transcripts induced or repressed by Ind+GSK was still greater than with indacaterol alone. A simple explanation of these data is that by maintaining the cAMP signal, PDE4 inhibitors likewise sustain gene transcription. However, GSK 256066 did not prolong the expression of all LABA-induced genes equally; in fact, for some genes the $AUC_{0\text{-}18h}$ was unaffected or even decreased by GSK 256066. Thus, additional mechanisms that accommodate variable effects of PDE4 inhibition on gene expression kinetics must be entertained. One possibility is that the initial and delayed components of gene induction are regulated by temporally distinct transcriptional events that involve feed forward loops (Mangan and Alon, 2003). This type of regulation has been described for many genes including *DUSP1* (Lu et al., 2008) and can equally explain both prolongation and retardation of gene expression kinetics.

**Genes with Therapeutic Potential.** The LABA- and LABA+PDE4 inhibitor-regulated transcriptomes in BEAS-2B cells contained genes that may help reduce exacerbation frequency and the associated inflammation (Perera et al., 2007) that characterises the COPD phenotype that responds to roflumilast. In particular, several up-regulated genes encode proteins that suppress pro-inflammatory cytokine

Molecular Pharmacology Fast Forward. Published on April 29, 2019 as DOI: 10.1124/mol.118.115311
This article has not been copyedited and formatted. The final version may differ from this version.



generation such as *CD200*, *DUSP1* and *SOCS3* (Liu et al., 2007; Snelgrove et al., 2008; Yoshimura et al., 2018), whereas others may directly protect against bacterial and viral exacerbations. For example, the multifunctional, secreted protein, DMBT1, binds Gram-positive and Gram-negative bacteria and so could defend against microbial pathogens; it also inhibits the infectivity of human influenza A and immunodeficiency viruses (Madsen et al., 2010). Likewise, *CRISPLD2* encodes a secreted lipopolysaccharide-binding protein (Wang et al., 2009) that can neutralise the pathogenicity of Gram-negative bacteria and, thereby, down-regulate TLR4-mediated inflammation (Zhang et al., 2016). LABAs and PDE4 inhibitors also induced several genes that may encode negative feedback regulators of inflammation that include *KLF2*, *KLF4*, *KLF15* and the NR4A family of transcription factors (Rodriguez-Calvo et al., 2017; Sweet et al., 2018). Many of these genes are further upregulated when a LABA and/or a PDE4 inhibitor are combined with a glucocorticoid (Moodley et al., 2013; Rider et al., 2018), which may be relevant to understanding how these drugs work in a clinical setting (Giembycz & Newton, 2014).

Noteworthy DEGs down-regulated by indacaterol and Ind+GSK include *EGR1*. This gene is induced by cigarette smoke and is elevated in the lungs of subjects with severe COPD (Ning et al., 2004) with potential to promote mucus hypersecretion (Wang et al., 2017), inflammation, fibrosis and remodelling in the airways (Cho et al., 2006; Lee et al., 2004). *TXNIP* is another cigarette smoke-sensitive gene (Sun et al., 2018) that may contribute to the free radical burden that often prevails in COPD airways (Domej et al., 2014) by encoding an inhibitor of the oxidoreductase, thioredoxin 1 (Nishiyama et al., 1999). Therefore, the ability of PDE4 inhibitors and LABAs to repress *EGR1* and *TXNIP* could help arrest pro-inflammatory and fibrotic changes in the lungs and reduce oxidative stress, respectively.

**Adverse-Effect Genes.** Chronic, $\beta_2$-adrenoceptor agonist monotherapy in asthma is associated with an increased risk of serious AEs (Cates et al., 2014; Pearce et al., 1991). The apparent *absence* of similar toxicity in subjects with COPD is, therefore, a paradox (Decramer et al., 2013). If genomic mechanisms contribute to these AEs in asthma as previously proposed (Ritchie et al., 2018; Yan et al., 2018), then how can these discrepant responses to treatment be rationalised? This question is pertinent given that the expression of putative AE genes was exaggerated by a PDE4 inhibitor. The profound differences in

aetiology, pathogenesis, inflammation and causes of exacerbations between the two diseases may provide an explanation (Decramer et al., 2013) such that these gene expression changes in COPD have less pathological relevance than in asthma. Alternatively, cells exposed chronically to cigarette smoke in a Th1-like inflammatory environment may respond to a LABA by expressing a less harmful transcriptome.

**Conclusions.** The results of this study implicate widespread changes in gene expression in the mechanism of action of PDE4 inhibitors in COPD. This effect may be particularly relevant when added on to a LABA or an ICS/LABA combination therapy. Nevertheless, a comparable genomic signature must be confirmed in airway epithelia harvested from individuals with COPD if this assertion to gain traction. Such *in vivo* investigations are necessary because they will reveal the genomic capacity of these drugs at therapeutically-relevant doses on a background of airways and extrapulmonary inflammation that is common in individuals exposed chronically to cigarette smoke. They will also provide valuable information on the extent to which cultured airway epithelial cells predict the genomic behaviour of their *in vivo* counterparts in response to drug interventions under pathological conditions. Finally, the anti-inflammatory activity of oral apremilast in plaque psoriasis and psoriatic arthritis suggests that systemic exposure could contribute to the mechanism of action of roflumilast and may help explain why inhaled PDE4 inhibitors are inactive in COPD.

Molecular Pharmacology Fast Forward. Published on April 29, 2019 as DOI: 10.1124/mol.118.115311
This article has not been copyedited and formatted. The final version may differ from this version.



## Acknowledgements

The authors acknowledge Sylvia Wilson for generating the RNA samples used for microarray-based gene expression profiling and Dr. Paul M. K. Gordon, Centre for Health Genomics and Informatics, University of Calgary for assistance with bioinformatics.

## Authorship Contributions

**Participated in research design:** Giembycz, Hamed, Newton, R. Joshi, Yan

**Conducted experiments:** Hamed, T Joshi, R Joshi, Yan

**Performed data analysis:** Giembycz, Hamed, T Joshi, R. Joshi, Mostafa, Yan

**Wrote, reviewed or edited the manuscript:** Giembycz, Hamed, T Joshi, R Joshi, Mostafa, Newton, Yan

Molecular Pharmacology Fast Forward. Published on April 29, 2019 as DOI: 10.1124/mol.118.115311
This article has not been copyedited and formatted. The final version may differ from this version.



## References

BinMahfouz H, Borthakur B, Yan D, George T, Giembycz MA and Newton R (2015) Superiority of combined phosphodiesterase (PDE)3/PDE4 inhibition over PDE4 inhibition alone on glucocorticoid- and long-acting $\beta_2$-adrenoceptor agonist-induced gene expression in human airway epithelial cells. *Mol Pharmacol* **87**:64-76.

Black JW and Leff P (1983) Operational models of pharmacological agonism. *Proc R Soc Lond B Biol Sci* **220**:141-162.

Bray NL, Pimentel H, Melsted P and Pachter L (2016) Near-optimal probabilistic RNA-seq quantification. *Nat Biotechnol* **34**:525-527.

Calverley PM, Rabe KF, Goehring UM, Kristiansen S, Fabbri LM and Martinez FJ (2009) Roflumilast in symptomatic chronic obstructive pulmonary disease: two randomised clinical trials. *Lancet* **374**:685-694.

Cates CJ, Wieland LS, Oleszczuk M and Kew KM (2014) Safety of regular formoterol or salmeterol in adults with asthma: an overview of Cochrane reviews. *Cochrane Database Syst Rev*:CD010314.

Cho SJ, Kang MJ, Homer RJ, Kang HR, Zhang X, Lee PJ, Elias JA and Lee CG (2006) Role of early growth response-1 (Egr-1) in interleukin-13-induced inflammation and remodeling. *J Biol Chem* **281**:8161-8168.

Cornbleet PJ and Gochman N (1979) Incorrect least-squares regression coefficients in method-comparison analysis. *Clin Chem* **25**:432-438.

Crystal RG (2014) Airway basal cells. The "smoking gun" of chronic obstructive pulmonary disease. *Am J Respir Crit Care Med* **190**:1355-1362.

Decramer ML, Hanania NA, Lotvall JO and Yawn BP (2013) The safety of long-acting $\beta_2$-agonists in the treatment of stable chronic obstructive pulmonary disease. *Int J Chron Obstruct Pulmon Dis* **8**:53-64.

Deyrup MD, Greco PG, Otero DH, Dennis DM, Gelband CH and Baker SP (1998) Irreversible binding of a carbostyril-based agonist and antagonist to the beta-adrenoceptor in $DDT_1$ MF-2 cells and rat aorta. *Br J Pharmacol* **124**:165-175.

Domej W, Oettl K and Renner W (2014) Oxidative stress and free radicals in COPD - implications and relevance for treatment. *Int J Chron Obstruct Pulmon Dis* **9**:1207-1224.

Gamble E, Grootendorst DC, Brightling CE, Troy S, Qiu Y, Zhu J, Parker D, Matin D, Majumdar S, Vignola AM, et al. (2003) Anti-inflammatory effects of the phosphodiesterase 4 inhibitor cilomilast (*Ariflo*) in chronic obstructive pulmonary disease. *Am J Respir Crit Care Med* **168**:976-982.

Giembycz MA (2008) Can the anti-inflammatory potential of PDE4 inhibitors be realized: guarded optimism or wishful thinking? *Br J Pharmacol* **155**:288-290.

Giembycz MA and Field SK (2010) Roflumilast: first phosphodiesterase 4 inhibitor approved for treatment of COPD. *Drug Des Devel Ther* **4**:147-158.

Giembycz MA and Maurice DH (2014) Cyclic nucleotide-based therapeutics for chronic obstructive pulmonary disease. *Curr Opin Pharmacol* **16**:89-107.

Giembycz MA and Newton R (2011) Harnessing the clinical efficacy of phosphodiesterase 4 inhibitors in inflammatory lung diseases: dual-selective phosphodiesterase inhibitors and novel combination therapies. *Handb Exp Pharmacol* **204**:415-446.

Giembycz MA and Newton R (2014) How phosphodiesterase 4 inhibitors work in patients with chronic obstructive pulmonary disease of the severe, bronchitic, frequent exacerbator phenotype. *Clin Chest Med* **35**:203-217.

Giembycz MA and Newton R (2015) Potential mechanisms to explain how LABAs and PDE4 inhibitors enhance the clinical efficacy of glucocorticoids in inflammatory lung diseases. *F1000Prime Rep* **7**:16.

Greer S, Page CW, Joshi T, Yan D, Newton R and Giembycz MA (2013) Concurrent agonism of adenosine $A_{2B}$ and glucocorticoid receptors in human airway epithelial cells cooperatively induces genes with anti-inflammatory potential: a novel approach to treat chronic obstructive pulmonary disease. *J Pharmacol Exp Ther* **346**:473-485.

Grootendorst DC, Gauw SA, Baan R, Kelly J, Murdoch RD, Sterk PJ and Rabe KF (2003) Does a single dose of the phosphodiesterase 4 inhibitor, cilomilast (15 mg), induce bronchodilation in patients with chronic obstructive pulmonary disease? *Pulm Pharmacol Ther* **16**:115-120.

Grootendorst DC, Gauw SA, Verhoosel RM, Sterk PJ, Hospers JJ, Bredenbroker D, Bethke TD, Hiemstra PS and Rabe KF (2007) Reduction in sputum neutrophil and eosinophil numbers by the PDE4 inhibitor roflumilast in patients with COPD. *Thorax* **62**:1081-1087.

Gross NJ, Giembycz MA and Rennard SI (2010) Treatment of chronic obstructive pulmonary disease with roflumilast, a new phosphodiesterase 4 inhibitor. *COPD* **7**:141-153.

Huang W, Sherman BT and Lempicki RA (2009) Systematic and integrative analysis of large gene lists using DAVID bioinformatics resources. *Nat Protoc* **4**:44-57.

Hatzelmann A, Morcillo EJ, Lungarella G, Adnot S, Sanjar S, Beume R, Schudt C and Tenor H (2010) The preclinical pharmacology of roflumilast - a selective, oral phosphodiesterase 4 inhibitor in development for chronic obstructive pulmonary disease. *Pulm Pharmacol Ther* **23**:235-256.

Joshi T, Yan D, Hamed O, Tannheimer SL, Phillips GB, Wright CD, Kim M, Salmon M, Newton R and Giembycz MA (2017) GS-5759, a bifunctional $\beta_2$-adrenoceptor agonist and phosphodiesterase 4 inhibitor for chronic obstructive pulmonary disease with a unique mode of action: effects on gene expression in human airway epithelial cells. *J Pharmacol Exp Ther* **360**:324-340.

Kaur M, Chivers JE, Giembycz MA and Newton R (2008) Long-acting $\beta_2$-adrenoceptor agonists synergistically enhance glucocorticoid-dependent transcription in human airway epithelial and smooth muscle cells. *Mol Pharmacol* **73**:203-214.

Kenakin T (2016) The mass action equation in pharmacology. *Br J Clin Pharmacol* **81**:41-51.

Lee CG, Cho SJ, Kang MJ, Chapoval SP, Lee PJ, Noble PW, Yehualaeshet T, Lu B, Flavell RA, Milbrandt J, et al. (2004) Early growth response gene 1-mediated apoptosis is essential for transforming growth factor β1-induced pulmonary fibrosis. *J Exp Med* **200**:377-389.

Leff P, Prentice DJ, Giles H, Martin GR and Wood J (1990) Estimation of agonist affinity and efficacy by direct, operational model-fitting. *J Pharmacol Methods* **23**:225-237.

Lew M (2007) Good statistical practice in pharmacology. Problem 2. *Br J Pharmacol* **152**:299-303.

Liu Y, Shepherd EG and Nelin LD (2007) MAPK phosphatases - regulating the immune response. *Nat Rev Immunol* **7**:202-212.

Lu TC, Wang Z, Feng X, Chuang P, Fang W, Chen Y, Neves S, Maayan A, Xiong H, Liu Y, et al. (2008) Retinoic acid utilizes CREB and USF1 in a transcriptional feed-forward loop in order to stimulate MKP1 expression in human immunodeficiency virus-infected podocytes. *Mol Cell Biol* **28**:5785-5794.

Madsen J, Mollenhauer J and Holmskov U (2010) Gp-340/DMBT1 in mucosal innate immunity. *Innate Immun* **16**:160-167.

Mangan S and Alon U (2003) Structure and function of the feed-forward loop network motif. *Proc Natl Acad Sci USA* **100**:11980-11985.

Martinez FJ, Calverley PM, Goehring UM, Brose M, Fabbri LM and Rabe KF (2015) Effect of roflumilast on exacerbations in patients with severe chronic obstructive pulmonary disease uncontrolled by combination therapy (REACT): a multicentre randomised controlled trial. *Lancet* **385**:857-866.

Martinez FJ, Rabe KF, Calverley PMA, Fabbri LM, Sethi S, Pizzichini E, McIvor A, Anzueto A, Alagappan VKT, Siddiqui S, et al. (2018) Determinants of response to roflumilast in severe COPD: Pooled analysis of two randomized trials. *Am J Respir Crit Care Med* **198**: 1268–1278.

Meja KK, Catley MC, Cambridge LM, Barnes PJ, Lum H, Newton R and Giembycz MA (2004) Adenovirus-mediated delivery and expression of a cAMP-dependent protein kinase inhibitor gene to BEAS-2B epithelial cells abolishes the anti-inflammatory effects of rolipram, salbutamol, and prostaglandin $E_2$: a comparison with H-89. *J Pharmacol Exp Ther* **309**:833-844.

Moodley T, Wilson SM, Joshi T, Rider CF, Sharma P, Yan D, Newton R and Giembycz MA (2013) Phosphodiesterase 4 inhibitors augment the ability of formoterol to enhance glucocorticoid-dependent gene transcription in human airway epithelial cells: a novel mechanism for the clinical efficacy of roflumilast in severe chronic obstructive pulmonary disease. *Mol Pharmacol* **83**:894-906.

Ning W, Li CJ, Kaminski N, Feghali-Bostwick CA, Alber SM, Di YP, Otterbein SL, Song R, Hayashi S, Zhou Z, et al. (2004) Comprehensive gene expression profiles reveal pathways related to the pathogenesis of chronic obstructive pulmonary disease. *Proc Natl Acad Sci USA* **101**:14895-14900.

Nishiyama A, Matsui M, Iwata S, Hirota K, Masutani H, Nakamura H, Takagi Y, Sono H, Gon Y and Yodoi J (1999) Identification of thioredoxin-binding protein-2/vitamin $D_3$ up-regulated protein 1 as a negative regulator of thioredoxin function and expression. *J Biol Chem* **274**:21645-21650.

Pearce N, Crane J, Burgess C, Jackson R and Beasley R (1991) Beta agonists and asthma mortality: *déjà vu*. *Clin Exp Allergy* **21**:401-410.

Penn RB, Bond RA and Walker JK (2014) GPCRs and arrestins in airways: implications for asthma. *Handb Exp Pharmacol* **219**:387-403.

Perera WR, Hurst JR, Wilkinson TM, Sapsford RJ, Mullerova H, Donaldson GC and Wedzicha JA (2007) Inflammatory changes, recovery and recurrence at COPD exacerbation. *Eur Respir J* **29**:527-534.

Pimentel H, Bray NL, Puente S, Melsted P and Pachter L (2017) Differential analysis of RNA-seq incorporating quantification uncertainty. *Nat Methods* **14**:687-690.

Pincelli C, Schafer PH, French LE, Augustin M and Krueger JG (2018) Mechanisms underlying the clinical effects of apremilast for psoriasis. *J Drugs Dermatol* **17**:835-840.

Rabe KF, Giembycz MA, Dent G, Perkins RS, Evans P and Barnes PJ (1993) Salmeterol is a competitive antagonist at β-adrenoceptors mediating inhibition of respiratory burst in guinea-pig eosinophils. *Eur J Pharmacol* **231**: 305-308.

Rider CF, Altonsy MO, Mostafa MM, Shah SV, Sasse S, Manson ML, Yan D, Karrman-Mardh C, Miller-Larsson A, Gerber AN, et al. (2018) Long-acting $\beta_2$-adrenoceptor agonists enhance glucocorticoid receptor (GR)-mediated transcription by gene-specific mechanisms rather than generic effects via GR. *Mol Pharmacol* **94**:1031-1046.

Ritchie AI, Singanayagam A, Wiater E, Edwards MR, Montminy M and Johnston SL (2018) $\beta_2$-Agonists enhance asthma-relevant inflammatory mediators in human airway epithelial cells. *Am J Respir Cell Mol Biol* **58**:128-132.

Rodriguez-Calvo R, Tajes M and Vazquez-Carrera M (2017) The NR4A subfamily of nuclearreceptors: potential new therapeutic targets for the treatment of inflammatory diseases. *Expert Opin Ther Targets* **21**:291-304.

Snelgrove RJ, Goulding J, Didierlaurent AM, Lyonga D, Vekaria S, Edwards L, Gwyer E, Sedgwick JD, Barclay AN and Hussell T (2008) A critical function for CD200 in lung immune homeostasis and the severity of influenza infection. *Nat Immunol* **9**:1074-1083.

Sun Q, Xu H, Xue J, Yang Q, Chen C, Yang P, Han A, Tu Q, Lu J, Gao X, et al. (2018) MALAT1 via microRNA-17 regulation of insulin transcription is involved in the dysfunction of pancreatic beta-cells induced by cigarette smoke extract. *J Cell Physiol* **233**: 8862-8873.

Sweet DR, Fan L, Hsieh PN and Jain MK (2018) Kruppel-like factors in vascular inflammation: mechanistic insights and therapeutic potential. *Front Cardiovasc Med* **5**:6.

Tannheimer SL, Wright CD and Salmon M (2012) Combination of roflumilast with a $\beta_2$-adrenergic receptor agonist inhibits proinflammatory and profibrotic mediator release from human lung fibroblasts. *Respir Res* **13**:28.

Tralau-Stewart CJ, Williamson RA, Nials AT, Gascoigne M, Dawson J, Hart GJ, Angell AD, Solanke YE, Lucas FS, Wiseman J, et al. (2011) GSK256066, an exceptionally high-affinity and selective inhibitor of phosphodiesterase 4 suitable for administration by inhalation: *in vitro*, kinetic, and *in vivo* characterization. *J Pharmacol Exp Ther* **337**:145-154.

Wang SB, Zhang C, Xu XC, Xu F, Zhou JS, Wu YP, Cao C, Li W, Shen HH, Cao JF, et al. (2017) Early growth response factor 1 is essential for cigarette smoke-induced MUC5AC expression in human bronchial epithelial cells. *Biochem Biophys Res Commun* **490**:147-154.

Wang ZQ, Xing WM, Fan HH, Wang KS, Zhang HK, Wang QW, Qi J, Yang HM, Yang J, Ren YN, et al. (2009) The novel lipopolysaccharide-binding protein CRISPLD2 is a critical serum protein to regulate endotoxin function. *J Immunol* **183**:6646-6656.

Wedzicha JA, Calverley PM and Rabe KF (2016) Roflumilast: a review of its use in the treatment of COPD. *Int J Chron Obstruct Pulmon Dis* **11**:81-90.

Wilson SM, Shen P, Rider CF, Traves SL, Proud D, Newton R and Giembycz MA (2009) Selective prostacyclin receptor agonism augments glucocorticoid-induced gene expression in human bronchial epithelial cells. *J Immunol* **183**:6788-6799.

Yan D, Hamed O, Joshi T, Mostafa MM, Jamieson KC, Joshi R, Newton R and Giembycz MA (2018) Analysis of the indacaterol-regulated transcriptome in human airway epithelial cells implicates gene expression changes in the adverse and therapeutic effects of $\beta_2$-adrenoceptor agonists. *J Pharmacol Exp Ther* **366**:220-236.

Yoshimura A, Ito M, Chikuma S, Akanuma T and Nakatsukasa H (2018) Negative regulation of cytokine signaling in immunity. *Cold Spring Harb Perspect Biol* **10**:a028571.

Zeller E, Stief HJ, Pflug B and Sastre-y-Hernandez M (1984) Results of a phase II study of the antidepressant effect of rolipram. *Pharmacopsychiatry* **17**:188-190.

Zhang H, Kho AT, Wu Q, Halayko AJ, Limbert Rempel K, Chase RP, Sweezey NB, Weiss ST and Kaplan F (2016) CRISPLD2 (LGL1) inhibits proinflammatory mediators in human fetal, adult, and COPD lung fibroblasts and epithelial cells. *Physiol Rep* **4**:e12942.

Zhang X, Odom DT, Koo SH, Conkright MD, Canettieri G, Best J, Chen H, Jenner R, Herbolsheimer E, Jacobsen E, et al. (2005) Genome-wide analysis of cAMP-response element binding protein occupancy, phosphorylation, and target gene activation in human tissues. *Proc Natl Acad Sci USA* **102**:4459-4464.

Molecular Pharmacology Fast Forward. Published on April 29, 2019 as DOI: 10.1124/mol.118.115311
This article has not been copyedited and formatted. The final version may differ from this version.



## Footnotes

This study was supported by a project grant from the Canadian Institutes for Health Research (PJT 152904), The Lung Association of Alberta & NWT and an unrestricted research grant from Gilead Sciences Inc, Seattle, USA. OH and TJ are recipients of studentships awarded by The Lung Association of Alberta & NWT. DY was supported by Alberta Innovates. Real-time PCR was facilitated by an equipment and infrastructure grant from the Canadian Fund of Innovation and the Alberta Science and Research Authority.

The authors state no conflict of interest.

[1]Current affiliation: Global Development Operations, Novartis Healthcare Pvt. Ltd. Salarpuria-Sattva Knowledge City, Raidurg, Hyderabad - 500 032, India.

Molecular Pharmacology Fast Forward. Published on April 29, 2019 as DOI: 10.1124/mol.118.115311
This article has not been copyedited and formatted. The final version may differ from this version.



## Figure Legends

**Fig. 1.** Relationships between indacaterol- and GSK 256066-regulated gene expression changes in BEAS-2B cells. Panel A: Deming regressions at 1, 2 and 6h between changes in the expression of all genes (by probe set) regulated by indacaterol (10nM) at FDRs of <1, <5 and <10% and their counterparts in cells treated with GSK 256066 (10nM). Induced or repressed probes sets are shown as red or blue circles, respectively, and are plotted as fold on a $\log_2$ scale where a value of 1 equates to baseline expression (horizontal and vertical dashed lines).Yellow circles represent genes that were validated by real-time PCR (Fig. 6; Supplemental Fig. 4). The letter in each yellow circle corresponds to a HGNC gene symbol and Affymetrix probe set ID code: **A.** *BMP2* (205289_at); **B.** *C5AR1* (220088_at); **C.** *CCL20* (205476_at); **D.** *CD200* (209582_s_at); **E.** *CRISPLD2* (221541_at); **F.** *DMBT1* (208250_s_at); **G.** *DUSP1* (201044_x_at); **H.** *FGFR2* (203638_at); **I.** *GAS1* (204456_s_at); **J.** *IL6* (205207_at); **K.** *NR4A2* (216248_s_at); **L.** *NR4A3* (209959_at); **M.** *PDE4D* (228962_at); **N.** *PDK4* (225702_at); **O.** *PRDM1* (228964_at); **P.** *RGS2* (202388_at); **Q.** *SGK1* (201739_at); **R.** *SOCS3* (206359_at); **S.** *EGR1* (227404_s_at); **T.** *TXNIP* (201008_s_at). Panel B: Correlations at 1, 2 and 6h of the changes in expression (in fold) of the same 18 genes (**A** to **R**) determined by microarray and PCR in BEAS-2B cells treated with GSK 256066 (10nM). Solid and dashed diagonal lines in each panel represent linear regression and the line-of-identity respectively.

**Fig. 2.** Comparative effects of indacaterol and Ind+GSK on the number of induced and repressed genes in BEAS-2B cells. Panel A: Time-course showing of the *number* of DEGs (>1.5-fold, <0.67-fold; FDR <10%) in cells treated for 1, 2, 6 and 18h with indacaterol (10nM), Ind+GSK (both 10nM) or vehicle. DEGs were identified using *Entrez Gene* and DAVID IDs and the number is shown in brackets at each time-point. Panel B: Proportional Venn diagrams showing the number of genes regulated by Ind+GSK (white set), indacaterol (black set) and both treatments (intersections) at each, and across all, time-points. See text for further details.

**Fig. 3.** Global effect of GSK 256066 on the indacaterol-induced transcriptome in BEAS-2B cells. Panels A-D: Genes (by probe set) that were significantly induced (>1-fold) by Ind+GSK at 1, 2, 6 and 18h at the FDR indicated were correlated against their counterparts in indacaterol-treated cells. The

Molecular Pharmacology Fast Forward. Published on April 29, 2019 as DOI: 10.1124/mol.118.115311
This article has not been copyedited and formatted. The final version may differ from this version.



black arrows in panels C and D indicate deviation from unity slope in favour of Ind+GSK (i.e. genes were induced more with Ind+GSK than with indacaterol alone). Panels E-H: Comparative global expression kinetics for the probe sets from panels A-D that were significantly upregulated by Ind+GSK at 1, 2, 6 and 18h, respectively with their counterparts in cells treated with indacaterol and GSK 256066 (areas shaded dark and light grey respectively). For example, in panel E, the global mean change in expression (in fold) of the 158 probe sets that were significantly upregulated by Ind+GSK at 1h was also calculated at the other three time-points, and at 1, 2, 6 and 18h in cells treated with indacaterol and GSK 256066. These calculations were replicated with the 519, 1055 and 39 probe sets that were significantly upregulated at 2, 6 and 18h (Panels F-H). The areas shaded green indicate the gain in $AUC_{0\text{-}18h}$ produced by Ind+GSK over indacaterol alone. The $AUC_{0\text{-}18h}$ for each intervention is indicated.

**Fig. 4.** Gene-dependent impact of PDE4 inhibition on the indacaterol $AUC_{0\text{-}18h}$ in BEAS-2B cells. The $AUC_{0\text{-}18h}$ of the 259 significantly up-regulated probe sets (FDR <10%; >2-fold at any time-point) were calculated in the absence and presence of GSK 256066 (10nM). The $AUC_{0\text{-}18h}^{Ind+GSK/Ind}$ are plotted on a linear scale as a heat map where red, blue and grey colours correspond to changes that are >1.1-fold (157 probe sets), <0.9-fold (34 probe sets) and from 0.9- to 1.1-fold (68 probe sets) respectively. Those genes validated by real-time PCR are shown on the right side of the panel where the letters assigned to HGNC symbols are consistent with the labelling used in figures 1 and 5 and in supplemental figures 2 and 3. *DNAI1* and *UGT1A8/9* represent genes at the extremes of this continuum where GSK 256066 maximally increased and decreased the indacaterol $AUC_{0\text{-}18h}$, respectively.

**Fig. 5.** Validation of the effect of GSK 256066 on gene induction kinetics produced by a maximally-effective concentration of indacaterol. BEAS-2B cells were treated for 1, 2, 6 and 18h with vehicle, GSK 256066 (GSK; 10nM), indacaterol (Ind; 10nM) and Ind+GSK (both 10nM). RNA was extracted and the expression of eighteen genes (selected from the 259 probe sets that were significantly induced by indacaterol, on the microarrays; Supplementary Table 6) was determined by real-time PCR. Gene expression changes were normalised to *GAPDH* and plotted as fold over time on a $\log_2$ scale where a value of 1 defines the baseline (dashed horizontal line). With the exception of *BMP2*, whose expression

Molecular Pharmacology Fast Forward. Published on April 29, 2019 as DOI: 10.1124/mol.118.115311
This article has not been copyedited and formatted. The final version may differ from this version.



kinetics in response to indacaterol was abbreviated by PDE4 inhibition, the green shaded areas indicate the gain in AUC produced by GSK 256066 when combined with indacaterol over indacaterol alone (shaded dark grey). The letters assigned to each HGNC gene symbol correspond to the same genes shown in figures 1 and 4 and in supplemental figures 2 and 3. Data represent the mean ± s.e. mean of *N* independent determinations.

**Fig. 6.** Effect of PDE4 inhibition on gene expression changes produced by submaximal concentrations of indacaterol and formoterol. Panel A: BEAS-2B cells were pre-treated (30min) with either GSK 256066 (GSK; 10nM) or roflumilast (Rof; 1μM) and then exposed to either indacaterol (Ind; 1nM) or formoterol (Form; 30pM**)** for an additional 1 and 2h. RNA was extracted and the expression of nine genes was determined by real-time PCR. Data were normalised to *GAPDH* and are presented as the mean ± s.e. mean of *N* independent determinations. Data were analysed by repeated measures, one-way ANOVA followed by Tukey's multiple comparisons test. **P*<0.05, significantly different from vehicle (V). $^{\#}P$<0.05, significantly different from LABA. Panel B: The 2h data from panel A expressed as fold changes in gene expression in response to LABA and PDE4 inhibitor in combination were correlated by the method of Pearson against the sum of the responses produced by each drug alone. These data were also subjected to Deming regression (black line) where black arrows indicate deviations from the lines of identity (diagonal dashed lines). Panel C: BEAS-2B cells were treated with vehicle (V) or GSK 256066 (GSK) and indacaterol (Ind) alone and in combination at the concentrations (in nM) indicated. At 6h, IL-6 was measured in supernatants by ELISA and the levels of NR4A2 and NR4A3 were determined in cell lysates by western blotting and expressed relative to *GAPDH*. Data are expressed as Box and Whisker plots of *N* independent determinations and were analysed by repeated measures, one-way ANOVA followed by Tukey's multiple comparisons test. **P*<0.05, significantly different from indacaterol. Representative westerns blots of NR4A2 and NR4A3 protein expression changes are also shown.

**Fig. 7.** Differential sensitivity of the LABA-regulated transcriptome to salmeterol. BEAS-2B cells were exposed to vehicle, $Salm_{0.3}$, $Salm_{0.5}$ and $Salm_{100}$ (to define maximum responses) for 2h and gene expression changes were determined by RNA-seq (*N* = 4 for each intervention). Panel A (left): The

Molecular Pharmacology Fast Forward. Published on April 29, 2019 as DOI: 10.1124/mol.118.115311
This article has not been copyedited and formatted. The final version may differ from this version.



change from vehicle in the expression of genes upregulated (≥2-fold; FDR ≤5%) by $Salm_{0.3}$ and $Salm_{0.5}$ were converted to a percentage of the counterpart $Salm_{100}$ data and presented as a heat map. The most (*TCF21*) and least (*NPTX1*) sensitive genes are indicated. Panel A (right): Simulated *E*/[A] curves were established for each salmeterol-induced gene from their respective $Salm_{0.3}/Salm_{100}$ values with $n_H$ constrained to a value of 1.8 (Supplemental Table 7). The degree to which each gene was upregulated by $Salm_{0.3}$ (as a percentage of its $Salm_{100}$ counterpart) is shown as a red circle on each *E*/[A] curve. Panel B: Salmeterol *E*/[A] curve data from supplemental figure 1 that define activation of the 6×CRE BEAS-2B reporter with $n_H$ = 1.8. Assuming that (i) salmeterol is a full agonist on all DEGs; (ii) changes in the expression of all DEGs are described by a symmetrical *E*/[A] curve with $n_H$ = 1.8; and (iii) $Salm_{100}$ maximally upregulated all DEGs, then the sensitivity between *NPTX1* and *TCF21* must differ by a factor of ~7.5-fold (grey circles) with $Salm_{0.3}$ being equivalent to $[A]_{11.6}$ and $[A]_{83}$ respectively. Panel C: BEAS-2B cells were incubated with vehicle (V) or RNO (1μM) and salmeterol (Salm; 100nM) alone and in combination. At 60min, the cells were lysed and cAMP measured by ELISA. Data are expressed as Box and Whisker plots of *N* independent determinations. Statistical analysis was by repeated measures, one-way ANOVA followed by Tukey's multiple comparisons test. **P*<0.05, significantly different from V. $^{\#}P$<0.05, significantly different from Salm.

**Fig. 8.** Effect of RNO on salmeterol-induced gene expression changes in BEAS-2B cells determined by RNA-seq. Panels A & B: Impact of RNO (1μM) on gene expression changes (≥2-fold; ≤0.5-fold; FDR ≤5%) induced by salmeterol after 2h exposure. The effects of $Salm_{0.3}$ + RNO and $Salm_{0.5}$ + RNO were correlated by the method of Pearson against the sum of the responses produced by each drug alone and expressed as a change in TPM from vehicle. The data were also subjected to Deming regression (black line) where the black arrows indicate deviation from the line-of-identity (diagonal dashed line). The panels shaded grey show the same data with *KRT17* excluded from the analyses. Red and blue circles represent induced and repressed genes, respectively. Panels C & D: Simulated *E*/[A] curves showing the effect of salmeterol alone and in the presence of RNO with $n_H$ constrained to a value of 1.8. In these examples, RNO produced a 3-fold sinistral displacement of the salmeterol *E*/[A] curve, which are shown in solid and dashed black respectively. Circles coloured blue and red show respectively the *fold*

Molecular Pharmacology Fast Forward. Published on April 29, 2019 as DOI: 10.1124/mol.118.115311
This article has not been copyedited and formatted. The final version may differ from this version.



((Salm + RNO)/Salm) and *percentage* difference ((Salm + RNO) - Salm) of salmeterol-induced responses (from -12 to -8M) produced by RNO plotted in 0.1 intervals of $\log_{10}$ concentration, which are described by a symmetrical bell-shaped curve. The greatest change in fold (6.47; from $[A]_{3.4}$ to $[A]_{22}$) and percentage difference (47%; from $[A]_{30}$ to $[A]_{77}$) were produced with salmeterol at 50pM (-10.3M) and 200pM (-9.7M) respectively. Panels E and F: Relationship between those genes induced by $Salm_{0.3}$ (expressed a percentage of the $Salm_{100}$ counterparts) and the degree to which the same gene was augmented by RNO given as a synergy index. This index is presented as a fold of the increase in TPM (i.e., $Salm_{0.3}$ + RNO/Σ($Salm_{0.3}$, RNO) - Vehicle (V)) in panel E and as a percentage difference (i.e., $Salm_{0.3}$ + RNO - (Σ($Salm_{0.3}$, RNO) - V)) in panel F after normalization to the $Salm_{100}$ data. Values above the horizontal dashed line in each panel indicate a synergistic interaction. Each upregulated gene (180 in total) is represented by a grey circle. Blue and red circles highlight *TCF21* and *NPTX1,* which lie towards the extremes of the sensitivity spectrum, with $Salm_{0.3}$ (-9.52M) being equal to $[A]_{83}$ and $[A]_{11.6}$ as indicated in figure 7C.

**Fig. 9.** Application of fractional, irreversible, $\beta_2$-adrenoceptor inactivation to determine the impact of PDE4 inhibition on the pharmacodynamics of LABA-induced gene expression. Panels A & C: *E*/[A] curves were constructed to salmeterol and β2A in the absence and presence of RNO (1μM) and GSK 256066 (10nM) respectively in 6×CRE BEAS-2B cells that had been pre-treated (60min) with vehicle or DCITC (100nM) and then washed in SFM. The two families of curves were analyzed by operational model fitting from which estimates of $K_A$, τ, *n*, $E_m$ and $p[A]_{50}$ (of the control curve) were derived (Table 1). The horizontal dashed lines represent baseline luciferase activity. The $K_A$ of each agonist was used to calculate the relationship between fractional $\beta_2$-adrenoceptor occupancy and reporter activation shown in panels B & D. The diagonal dashed line is the line-of-identity where luciferase activity is a linear function of receptor occupancy. Panels E-G: BEAS-2B cells were treated as described for the experiments shown in panels A-D. At 2h, RNA was harvested and real-time PCR performed for *CRISPLD2*, *NR4A2* and *RGS2*. The data were normalised to *GAPDH,* expressed as fold and used to construct *E*/[A] curves. Data represent the mean ± s.e. mean of *N* independent determinations.

Molecular Pharmacology Fast Forward. Published on April 29, 2019 as DOI: 10.1124/mol.118.115311
This article has not been copyedited and formatted. The final version may differ from this version.

**Table 1.** Effect of PDE4 inhibition on the pharmacodynamic parameters that define salmeterol- and β2A-induced CRE-dependent reporter activation in BEAS-2B cells.

| | | Parameter Estimates | | | | | | | | |
|---|---|---|---|---|---|---|---|---|---|---|
| **Treatment** | ***N*** | **p[A]$_{50}$** | **p[A']$_{50}$** | **p$K_A$** | **$K_A$/[A]$_{50}$** | **$K_A$/[A']$_{50}$** | **$E_m$ (fold)** | ***n*** | **logτ** | **logτ'** |
| Salmeterol | 6 | 9.33 ± 0.11 | 8.30 ± 0.04 | 8.43 ± 0.01 | 7.9 | 0.74 | 19.1 ± 0.5 | 2.01 ± 0.57 | 1.02 ± 0.10 | -0.04 ± 0.03 |
| Salmeterol + RNO | | 9.94 ± 0.13 | 8.63 ± 0.18 | | 32.4 | 1.59 | | | 1.38 ± 0.21 | 0.24 ± 0.10 |
| β2A | 6 | 8.67 ± 0.04 | 7.32 ± 0.06 | 7.39 ± 0.06 | 19.0 | 0.85 | 14.0 ± 0.8 | 1.50 ± 0.15 | 1.26 ± 0.07 | 0.10 ± 0.03 |
| β2A + GSK 256066 | | 9.00 ± 0.04 | 7.85 ± 0.05 | | 40.7 | 2.88 | | | 1.60 ± 0.09 | 0.38 ± 0.05 |

Agonist *E*/[A] curves in the absence and presence of PDE4 inhibitor were constructed in cells treated with or without DCITC (100nM for 60min). The four curves in each family were analysed simultaneously by operational model fitting. p[A]$_{50}$ and p[A']$_{50}$ refer to the concentration (-log$_{10}$ M) of agonist that produced half maximum response in the absence and presence of DCITC respectively. Logτ and logτ' values refer to the operational efficacy of $\beta_2$-adrenoceptor agonist before and after alkylation respectively. Parameters were derived from the data shown in figure 9A and C.

Figure 1

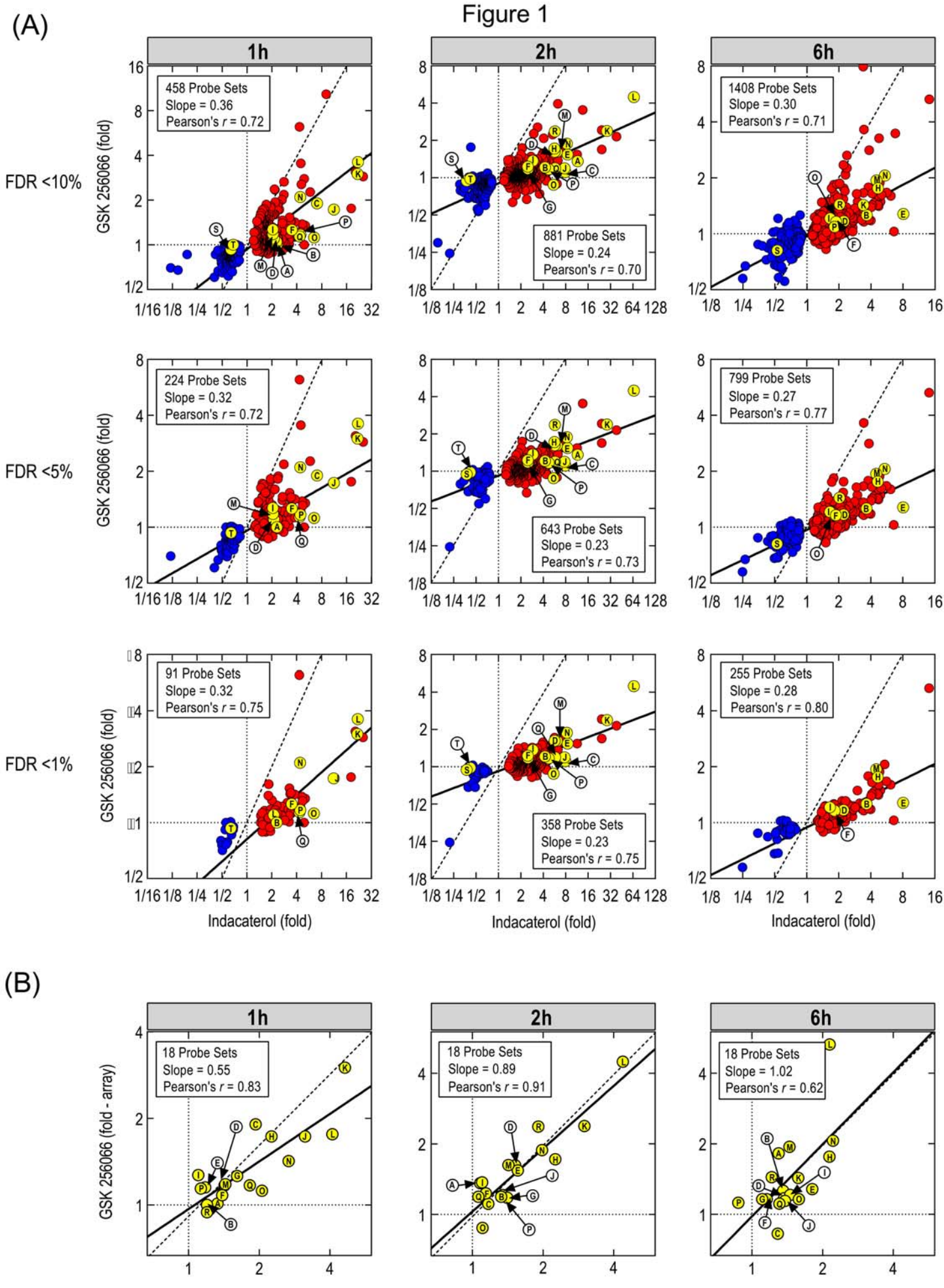
(A)
1h
2h
6h
FDR <10%
FDR <5%
FDR <1%
458 Probe Sets
Slope = 0.36
Pearson's r = 0.72
881 Probe Sets
Slope = 0.24
Pearson's r = 0.70
1408 Probe Sets
Slope = 0.30
Pearson's r = 0.71
224 Probe Sets
Slope = 0.32
Pearson's r = 0.72
643 Probe Sets
Slope = 0.23
Pearson's r = 0.73
799 Probe Sets
Slope = 0.27
Pearson's r = 0.77
91 Probe Sets
Slope = 0.32
Pearson's r = 0.75
358 Probe Sets
Slope = 0.23
Pearson's r = 0.75
255 Probe Sets
Slope = 0.28
Pearson's r = 0.80
GSK 256066 (fold)
Indacaterol (fold)
(B)
18 Probe Sets
Slope = 0.55
Pearson's r = 0.83
18 Probe Sets
Slope = 0.89
Pearson's r = 0.91
18 Probe Sets
Slope = 1.02
Pearson's r = 0.62
GSK 256066 (fold - array)
GSK 256066 (fold - PCR)

Figure 2

(A)

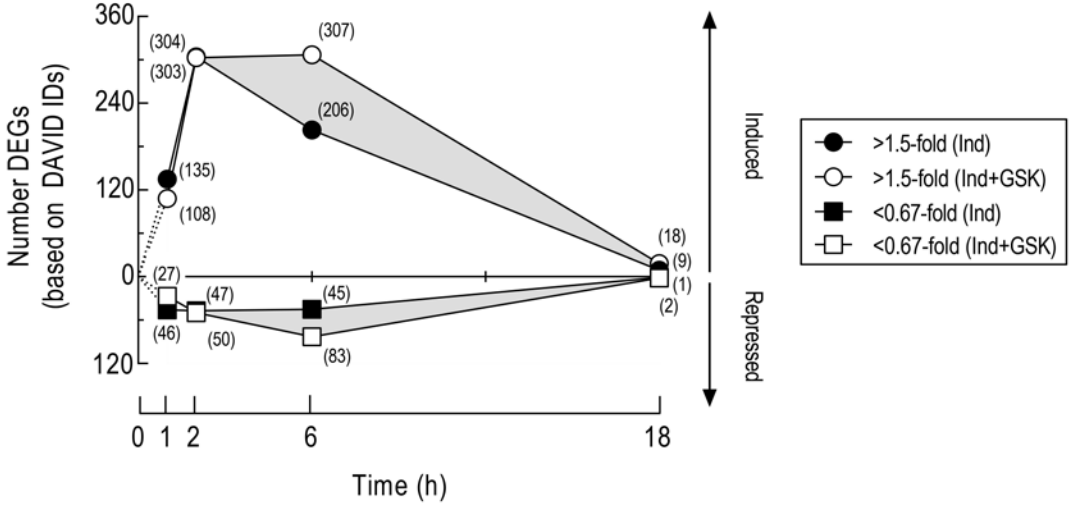
Number DEGs
(based on DAVID IDs)
360
240
120
0
120
(304)
(303)
(307)
(206)
(135)
(108)
(27)
(47)
(45)
(46)
(50)
(83)
(18)
(9)
(1)
(2)
Induced
Repressed
0 1 2 6 18
Time (h)
>1.5-fold (Ind)
>1.5-fold (Ind+GSK)
<0.67-fold (Ind)
<0.67-fold (Ind+GSK)

(B)

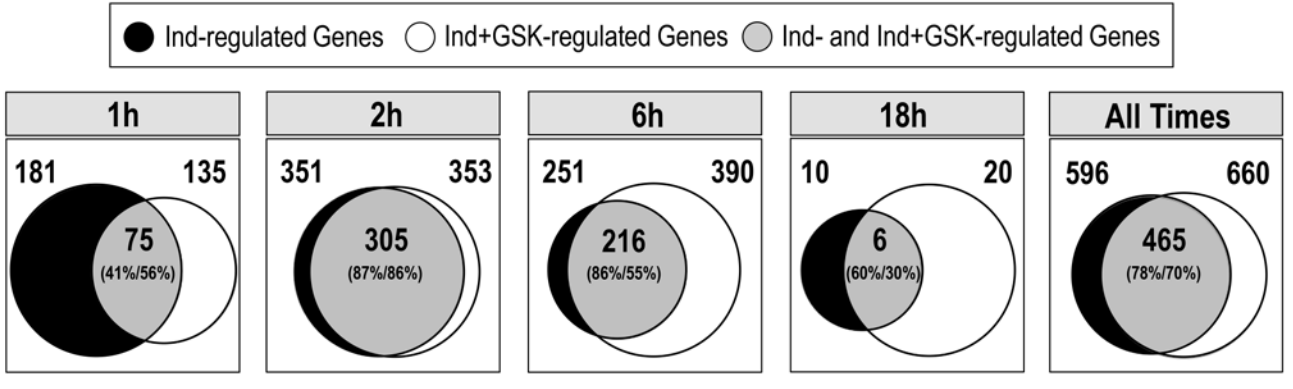
Ind-regulated Genes
Ind+GSK-regulated Genes
Ind- and Ind+GSK-regulated Genes
1h
181
135
75
(41%/56%)
2h
351
353
305
(87%/86%)
6h
251
390
216
(86%/55%)
18h
10
20
6
(60%/30%)
All Times
596
660
465
(78%/70%)

Figure 3

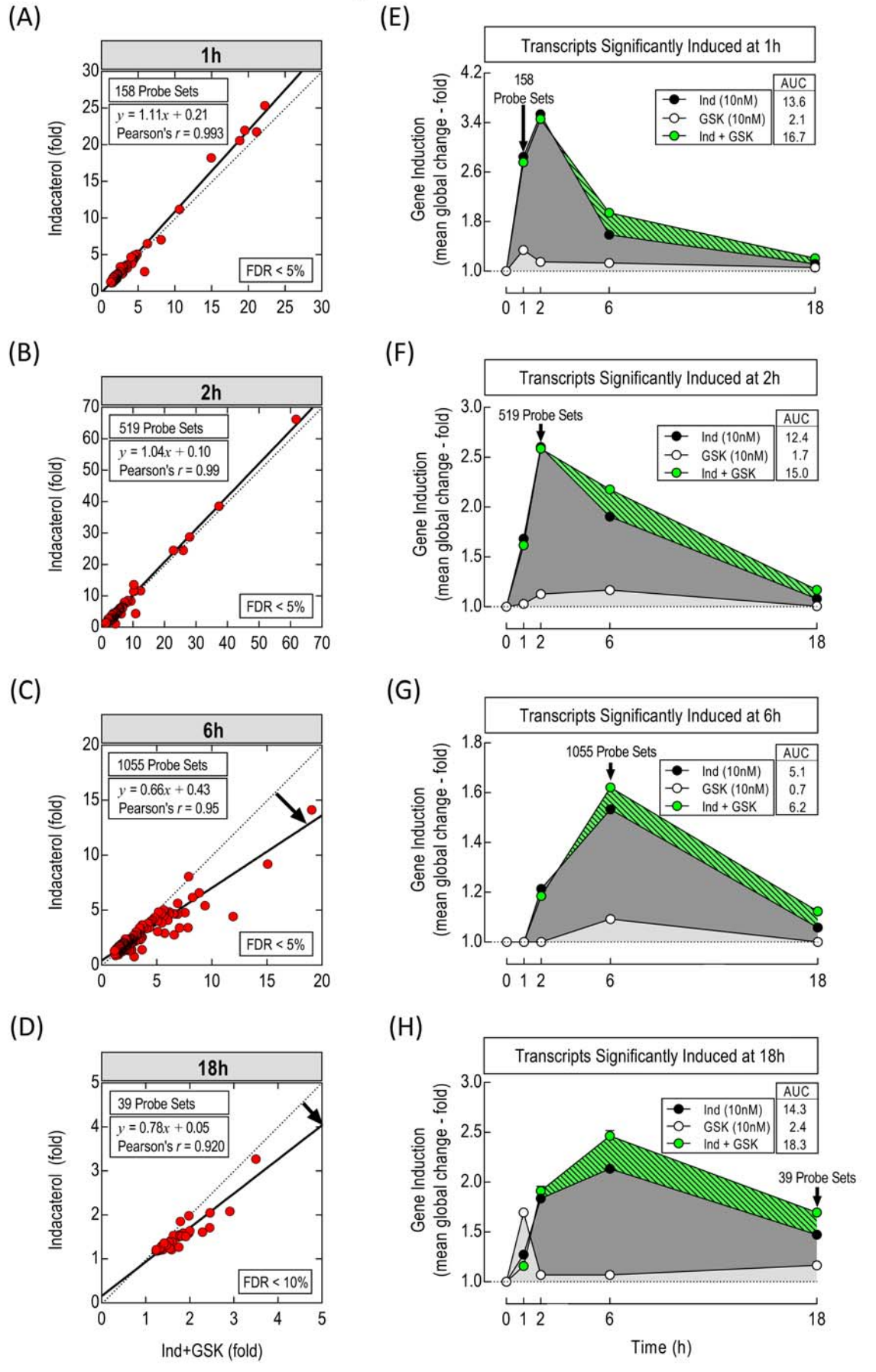
(A)
1h
158 Probe Sets
y = 1.11x + 0.21
Pearson's r = 0.993
FDR < 5%
Indacaterol (fold)
(B)
2h
519 Probe Sets
y = 1.04x + 0.10
Pearson's r = 0.99
FDR < 5%
Indacaterol (fold)
(C)
6h
1055 Probe Sets
y = 0.66x + 0.43
Pearson's r = 0.95
FDR < 5%
Indacaterol (fold)
(D)
18h
39 Probe Sets
y = 0.78x + 0.05
Pearson's r = 0.920
FDR < 10%
Indacaterol (fold)
Ind+GSK (fold)
(E)
Transcripts Significantly Induced at 1h
158
Probe Sets
AUC
Ind (10nM) 13.6
GSK (10nM) 2.1
Ind + GSK 16.7
Gene Induction
(mean global change - fold)
(F)
Transcripts Significantly Induced at 2h
519 Probe Sets
AUC
Ind (10nM) 12.4
GSK (10nM) 1.7
Ind + GSK 15.0
Gene Induction
(mean global change - fold)
(G)
Transcripts Significantly Induced at 6h
1055 Probe Sets
AUC
Ind (10nM) 5.1
GSK (10nM) 0.7
Ind + GSK 6.2
Gene Induction
(mean global change - fold)
(H)
Transcripts Significantly Induced at 18h
AUC
Ind (10nM) 14.3
GSK (10nM) 2.4
Ind + GSK 18.3
39 Probe Sets
Gene Induction
(mean global change - fold)
Time (h)

# Figure 4

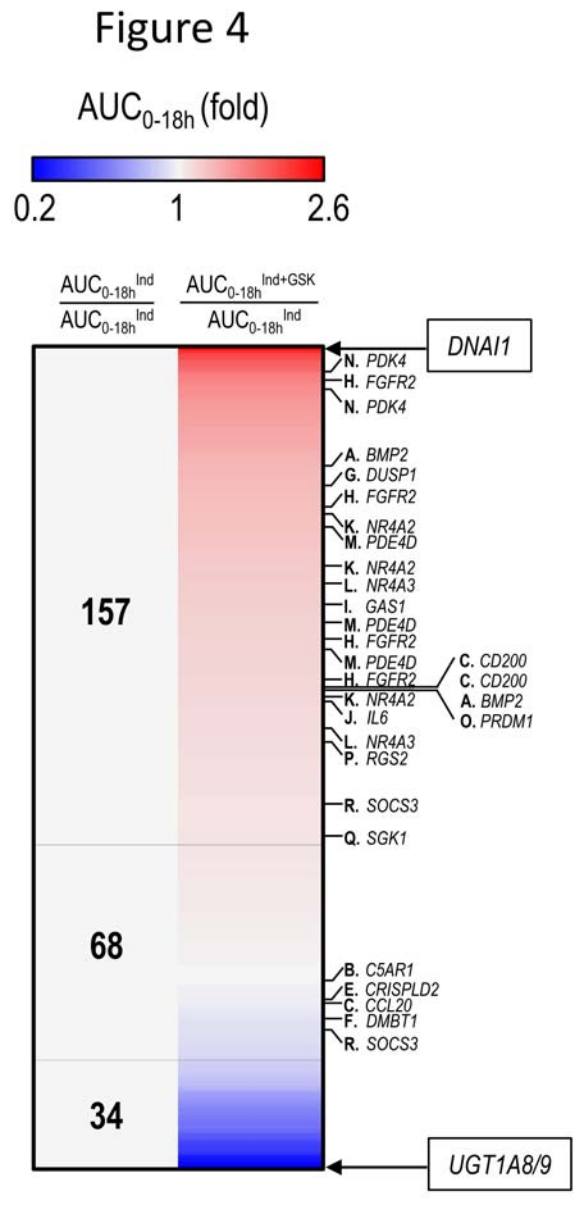
AUC0-18h (fold)
0.2
1
2.6
AUC0-18h Ind / AUC0-18h Ind
AUC0-18h Ind+GSK / AUC0-18h Ind
DNAI1
N. PDK4
H. FGFR2
N. PDK4
A. BMP2
G. DUSP1
H. FGFR2
K. NR4A2
M. PDE4D
K. NR4A2
L. NR4A3
I. GAS1
M. PDE4D
H. FGFR2
M. PDE4D
H. FGFR2
C. CD200
C. CD200
A. BMP2
O. PRDM1
K. NR4A2
J. IL6
L. NR4A3
P. RGS2
R. SOCS3
Q. SGK1
157
68
34
B. C5AR1
E. CRISPLD2
C. CCL20
F. DMBT1
R. SOCS3
UGT1A8/9

# Figure 5

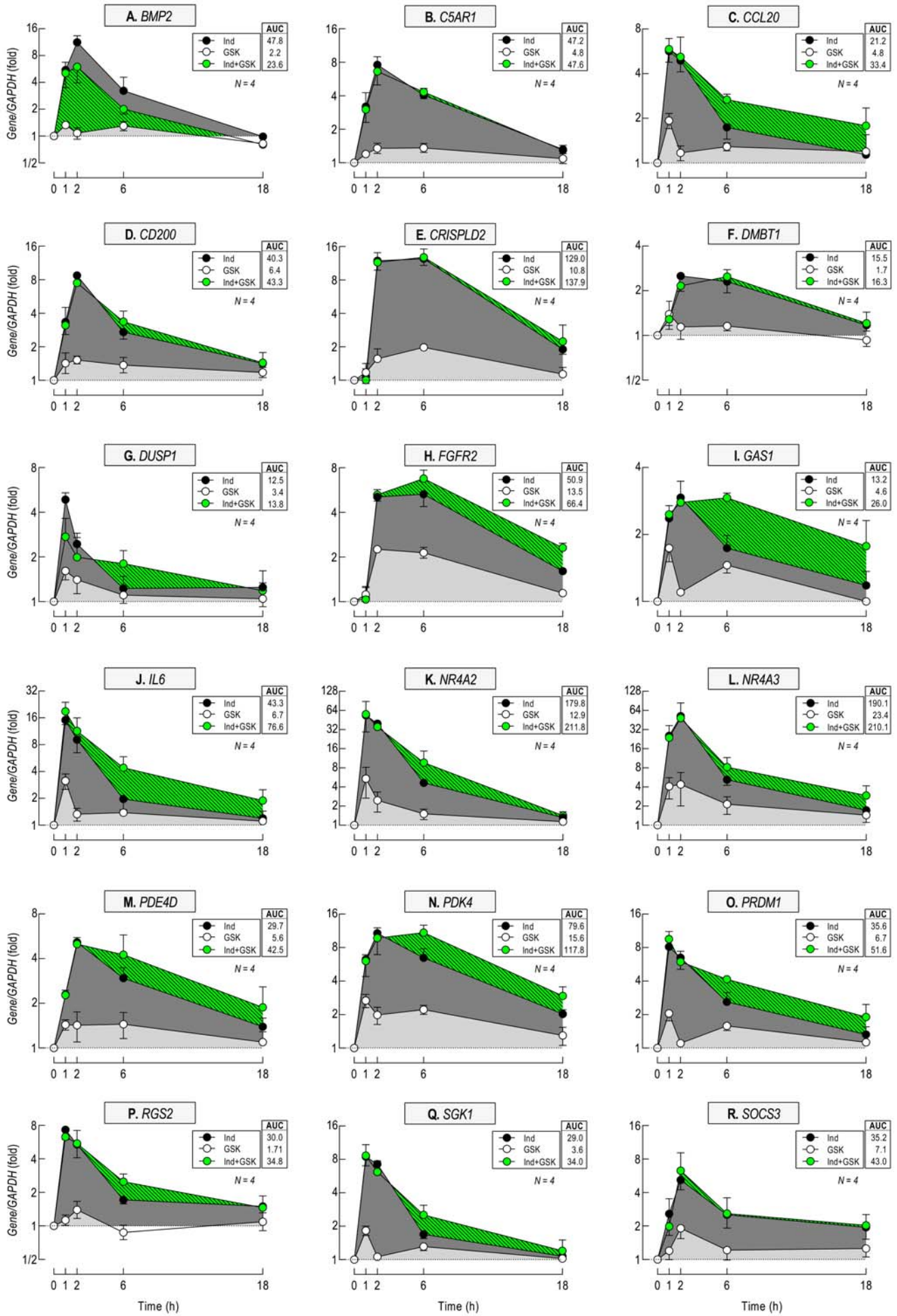
A. BMP2
Ind 47.8
GSK 2.2
Ind+GSK 23.6
N = 4
B. C5AR1
Ind 47.2
GSK 4.8
Ind+GSK 47.6
N = 4
C. CCL20
Ind 21.2
GSK 4.8
Ind+GSK 33.4
N = 4
D. CD200
Ind 40.3
GSK 6.4
Ind+GSK 43.3
N = 4
E. CRISPLD2
Ind 129.0
GSK 10.8
Ind+GSK 137.9
N = 4
F. DMBT1
Ind 15.5
GSK 1.7
Ind+GSK 16.3
N = 4
G. DUSP1
Ind 12.5
GSK 3.4
Ind+GSK 13.8
N = 4
H. FGFR2
Ind 50.9
GSK 13.5
Ind+GSK 66.4
N = 4
I. GAS1
Ind 13.2
GSK 4.6
Ind+GSK 26.0
N = 4
J. IL6
Ind 43.3
GSK 6.7
Ind+GSK 76.6
N = 4
K. NR4A2
Ind 179.8
GSK 12.9
Ind+GSK 211.8
N = 4
L. NR4A3
Ind 190.1
GSK 23.4
Ind+GSK 210.1
N = 4
M. PDE4D
Ind 29.7
GSK 5.6
Ind+GSK 42.5
N = 4
N. PDK4
Ind 79.6
GSK 15.6
Ind+GSK 117.8
N = 4
O. PRDM1
Ind 35.6
GSK 6.7
Ind+GSK 51.6
N = 4
P. RGS2
Ind 30.0
GSK 1.71
Ind+GSK 34.8
N = 4
Q. SGK1
Ind 29.0
GSK 3.6
Ind+GSK 34.0
N = 4
R. SOCS3
Ind 35.2
GSK 7.1
Ind+GSK 43.0
N = 4
AUC
Gene/GAPDH (fold)
Time (h)

# Figure 6

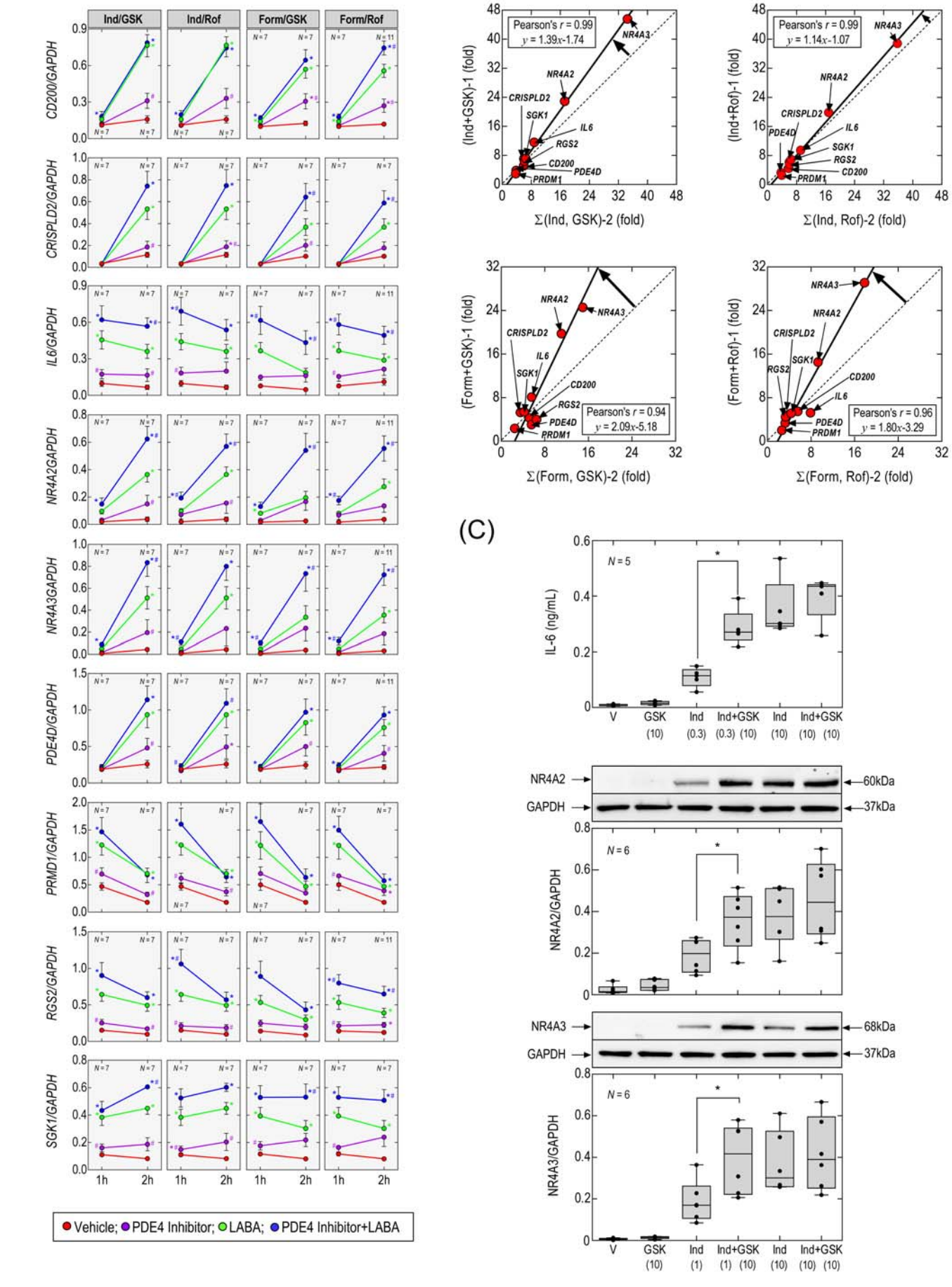
(A)
Ind/GSK
Ind/Rof
Form/GSK
Form/Rof
CD200/GAPDH
CRISPLD2/GAPDH
IL6/GAPDH
NR4A2GAPDH
NR4A3GAPDH
PDE4D/GAPDH
PRMD1/GAPDH
RGS2/GAPDH
SGK1/GAPDH
1h
2h
Vehicle; PDE4 Inhibitor; LABA; PDE4 Inhibitor+LABA
(B)
Pearson's r = 0.99
y = 1.39x-1.74
(Ind+GSK)-1 (fold)
Σ(Ind, GSK)-2 (fold)
Pearson's r = 0.99
y = 1.14x-1.07
(Ind+Rof)-1 (fold)
Σ(Ind, Rof)-2 (fold)
Pearson's r = 0.94
y = 2.09x-5.18
(Form+GSK)-1 (fold)
Σ(Form, GSK)-2 (fold)
Pearson's r = 0.96
y = 1.80x-3.29
(Form+Rof)-1 (fold)
Σ(Form, Rof)-2 (fold)
NR4A3
NR4A2
CRISPLD2
SGK1
IL6
RGS2
CD200
PDE4D
PRDM1
(C)
IL-6 (ng/mL)
N = 5
V
GSK (10)
Ind (0.3)
Ind+GSK (0.3) (10)
Ind (10)
Ind+GSK (10) (10)
NR4A2
GAPDH
60kDa
37kDa
NR4A2/GAPDH
N = 6
NR4A3
68kDa
NR4A3/GAPDH
Ind (1)
Ind+GSK (1) (10)

Figure 7

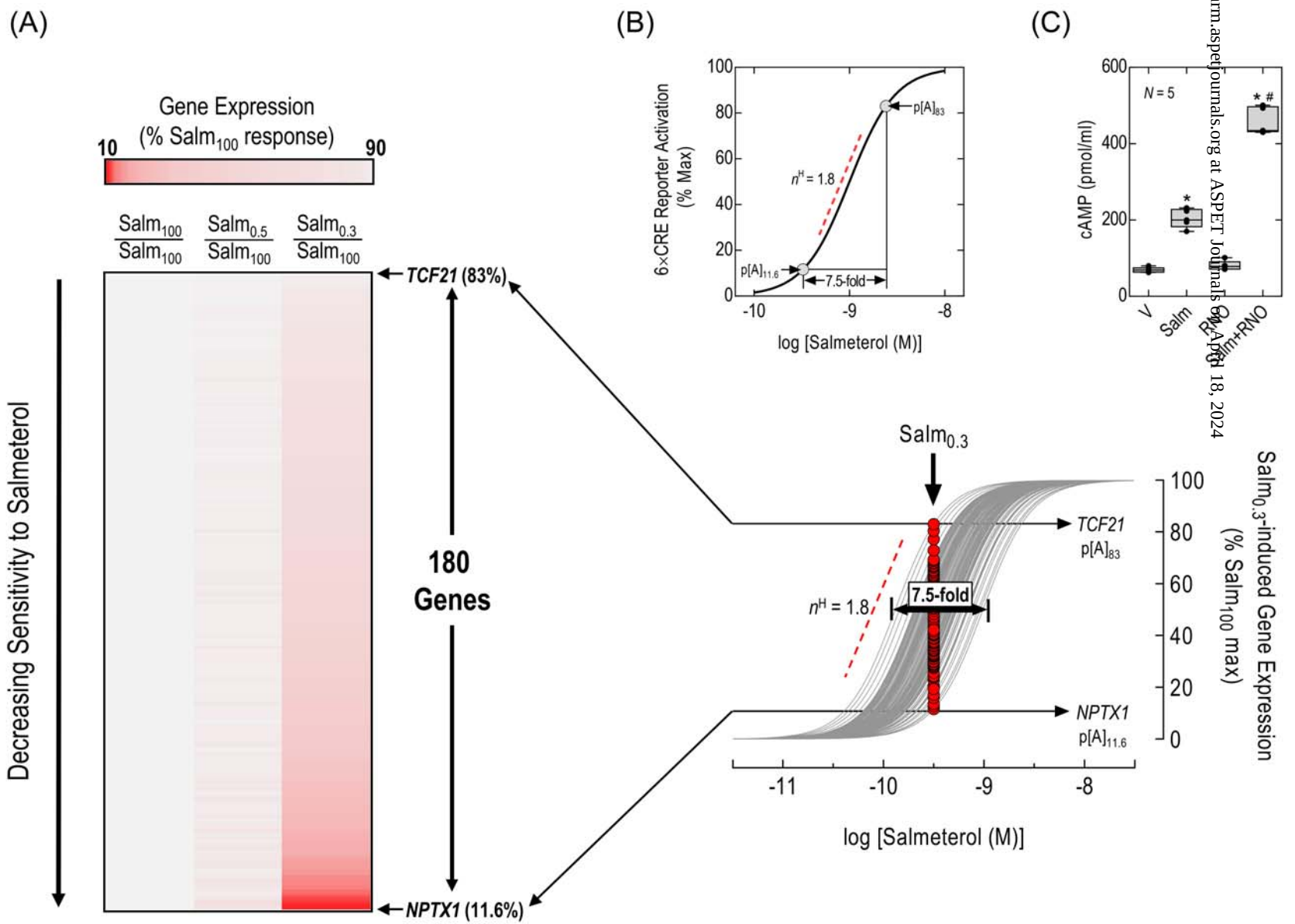

# Figure 8

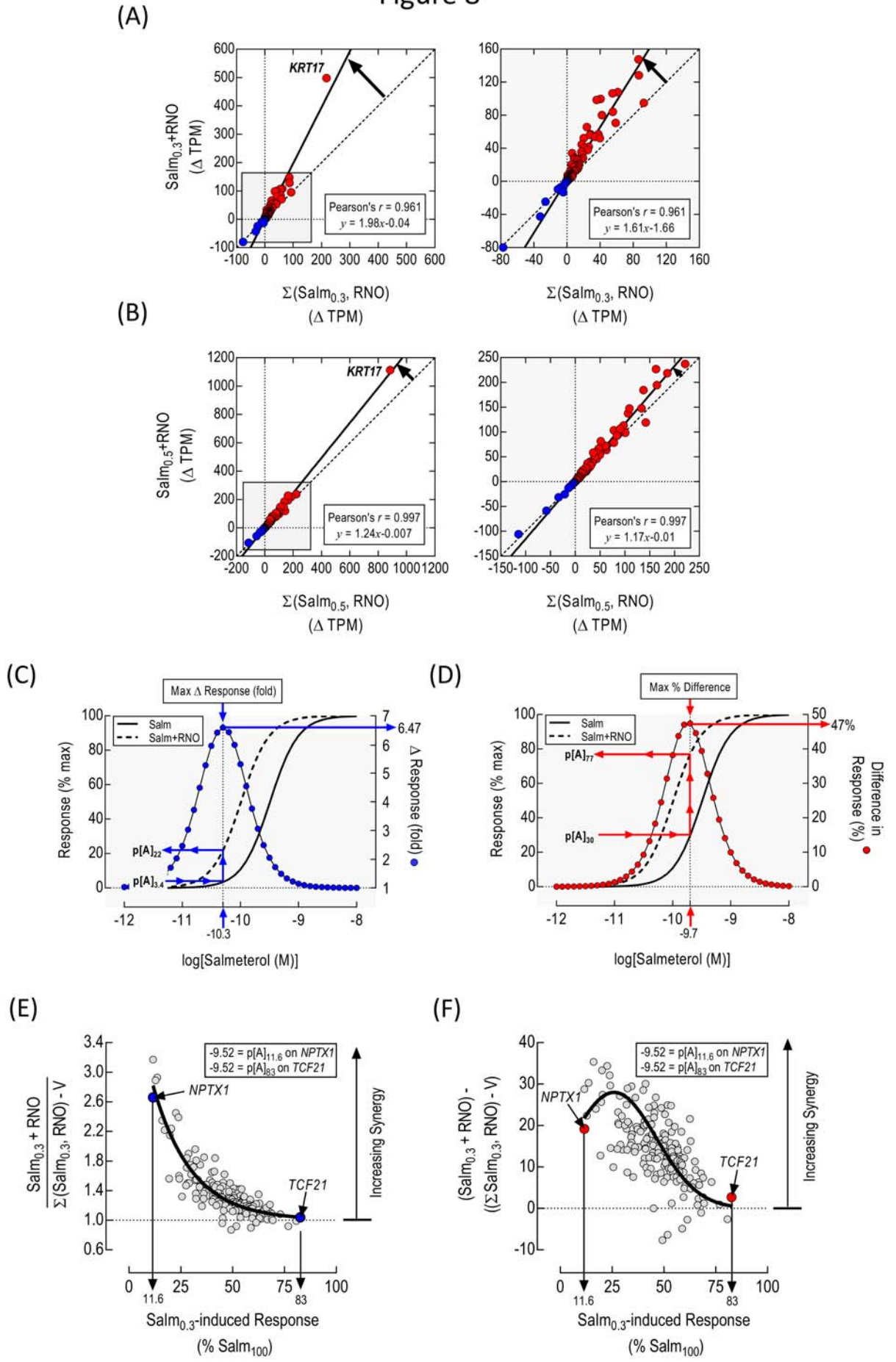
(A)
KRT17
Salm0.3+RNO (Δ TPM)
Pearson's r = 0.961
y = 1.98x-0.04
Σ(Salm0.3, RNO) (Δ TPM)
Pearson's r = 0.961
y = 1.61x-1.66
(B)
KRT17
Salm0.5+RNO (Δ TPM)
Pearson's r = 0.997
y = 1.24x-0.007
Σ(Salm0.5, RNO) (Δ TPM)
Pearson's r = 0.997
y = 1.17x-0.01
(C)
Max Δ Response (fold)
Salm
Salm+RNO
Response (% max)
Δ Response (fold)
6.47
p[A]22
p[A]3.4
-10.3
log[Salmeterol (M)]
(D)
Max % Difference
Salm
Salm+RNO
47%
p[A]77
p[A]30
Difference in Response (%)
-9.7
log[Salmeterol (M)]
(E)
-9.52 = p[A]11.6 on NPTX1
-9.52 = p[A]83 on TCF21
NPTX1
TCF21
Increasing Synergy
Salm0.3 + RNO / Σ(Salm0.3, RNO) - V
11.6
83
Salm0.3-induced Response (% Salm100)
(F)
-9.52 = p[A]11.6 on NPTX1
-9.52 = p[A]83 on TCF21
NPTX1
TCF21
Increasing Synergy
(Salm0.3 + RNO) - ((ΣSalm0.3, RNO) - V)
11.6
83
Salm0.3-induced Response (% Salm100)

# Figure 9

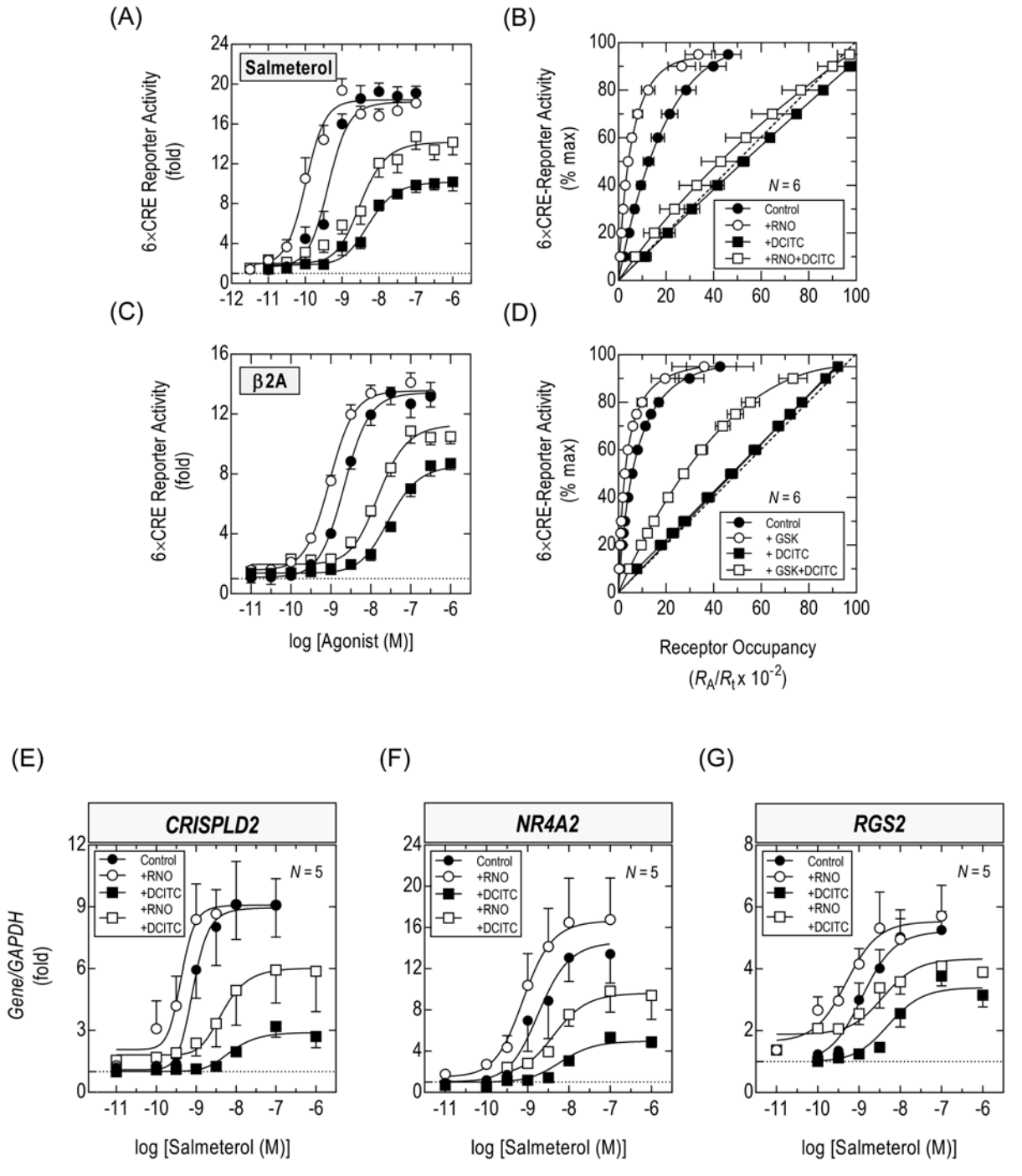
(A)
Salmeterol
6×CRE Reporter Activity (fold)
(B)
6×CRE-Reporter Activity (% max)
N = 6
Control
+RNO
+DCITC
+RNO+DCITC
(C)
β2A
6×CRE Reporter Activity (fold)
log [Agonist (M)]
(D)
6×CRE-Reporter Activity (% max)
N = 6
Control
+ GSK
+ DCITC
+ GSK+DCITC
Receptor Occupancy
($R_A/R_t$ x $10^{-2}$)
(E)
CRISPLD2
Gene/GAPDH (fold)
N = 5
Control
+RNO
+DCITC
+RNO
+DCITC
log [Salmeterol (M)]
(F)
NR4A2
N = 5
log [Salmeterol (M)]
(G)
RGS2
N = 5
log [Salmeterol (M)]